



Contents lists available at ScienceDirect

Journal of the Mechanics and Physics of Solids

journal homepage: www.elsevier.com/locate/jmps

Experiments and modeling of the viscoelastic behavior of polymeric gels

Nikola Bosnjak^a, Siva Nadimpalli^b, Dai Okumura^c, Shawn A. Chester^{a,*}^a Mechanical Engineering, New Jersey Institute of Technology, Newark, NJ 07102 USA^b Department of Mechanical Engineering, Michigan State University, East Lansing, MI 48824 USA^c Department of Mechanical Systems Engineering, Nagoya University, Nagoya, 464-8603, Japan

ARTICLE INFO

Article history:

Received 1 October 2019

Revised 13 December 2019

Accepted 14 December 2019

Available online 14 December 2019

ABSTRACT

A polymeric gel is a cross-linked polymer network swollen with a solvent. Also, as is well known many polymeric materials exhibit viscoelastic behavior in their mechanical response. In this work, we report on our recent experimental observations and theoretical modeling involving the change in the viscoelastic response of the polymeric material VHB caused by equilibrium swelling in multiple solvents. To characterize this change, we have developed an experimental procedure that includes mechanical testing when virgin, free swelling, mechanical testing when swollen, and mechanical testing after drying. A model is used to help interpret the experimental results. The key finding of this work is that our results indicate that the viscoelastic behavior of initially dry VHB, reversibly, becomes essentially hyperelastic when swollen to equilibrium in multiple solvents.

© 2019 Elsevier Ltd. All rights reserved.

1. Introduction

When exposed to a suitable solvent, many polymeric materials will imbibe the solvent. During this process, the polymer network expands, and the fluid molecules migrate into the polymer microstructure, forming a solid-fluid continuum known as polymeric gel. And many polymeric gels are classified as active materials due to their ability to respond to various stimuli.

Polymeric gels are found in a wide range of technologically relevant applications. Their responsiveness to environmental stimuli is utilized in soft robotics (Rus and Tolley, 2015), as well as in the oil industry where swellable elastomers are commonly employed as packers (Kleverlaan et al., 2005). Due to the similarity of gels with biological materials, polymeric gels are extensively used in tissue engineering (cf., e.g. Lutolf and Hubbell, 2005; Ronaldson-Bouchard et al., 2018). In addition, many polymeric gels are biocompatible and biodegradable, making them highly suitable for drug delivery applications (cf., e.g. Deligkaris et al., 2010; Zhang et al., 2015) and medical implants (Woerly et al., 2001).

The earliest research on the mixing behavior of gels and the seminal theories on polymer mixing are commonly considered to be the work of Flory (1942) and Huggins (1942). Shortly thereafter Flory and Rehner (1943a,b) extended that work to include the elasticity of a polymer network. Following that early work, a more contemporary resurgence into research on polymeric gels was initiated by Tanaka and Fillmore (1979). Recent years saw an extensive number of multiphysics continuum-level gel theories for the coupled diffusion-deformation behavior being developed (cf., e.g. Chester and Anand, 2010; Cohen and McMeeking, 2019; Doi, 2009; Duda et al., 2010; Hong et al., 2008; Lucantonio et al., 2013). Alongside

* Corresponding author.

E-mail address: shawn.a.chester@njit.edu (S.A. Chester).

the theoretical research, various experimental procedures have been developed to capture the mechanical behavior of gels, some of which include indentation (Hu et al., 2010), microscale tensile testing (Johnson et al., 2004) and compression testing (Farshad and Le Roux, 2005; Kean et al., 2014). Most of the above mentioned experimental procedures involve a small-scale deformation of the material. In addition, large deformation testing of gels is conducted by Rizzieri et al. (2003), Webber et al. (2007), and Yohsuke et al. (2011). Although the incorporation of large deformations is common in many modeling and computational studies, the insufficient amount of relevant experimental data is impeding research that would push our knowledge further.

A vast number of polymeric materials exhibit a non-linear viscoelastic behavior. Viscoelasticity in polymeric materials is commonly considered to arise due to the difference in time scale between rapid short-range motion and slower long-range motion of polymeric chains, as well as the interaction between the chains (Ferry, 1980). Being such a well known phenomena, the viscoelastic behavior of polymeric materials has been thoroughly researched over the past decades. Mechanical testing of viscoelastic polymers was performed by Smart and Williams (1972), Partom and Schanin (1983) and Hossain et al. (2012). Moreover, there have been many notable attempts to model the time-dependent behavior of viscoelastic polymers. Some of the initial work on modeling viscoelasticity in polymers was done by Green and Tobolsky (1946) and Biot (1954), followed by the models developed by Valanis (1966) and Crochet and Naghdi (1969). More recent constitutive models are the work of Drozdov (1997), Reese and Govindjee (1998), Bergström and Boyce (1998), Drozdov and Dorfmann (2002), Miehe and Göktepe (2005) and Linder et al. (2011).

The behavior of viscoelastic polymers is known to be affected by different environmental conditions, such as temperature, voltage, and chemical potential. Experimental data on temperature dependent viscoelastic behavior was published as early as mid 1950s (cf., e.g. Plazek, 1965; 1980; Williams et al., 1955) with some more recent observations by Khan and Lopez-Pamies (2002) and Drozdov et al. (2008). The vast amount of experimental research is accompanied by constitutive models to capture that behavior (Drozdov et al., 2008; Khan et al., 2006; Nguyen et al., 2008; Reese, 2003). In addition to studies on the electro-elasticity (cf., e.g. Cohen et al., 2017; Dorfmann and Ogden, 2005), the coupled electro-mechanical behavior of viscoelastic polymers has been shown and modeled in the literature (Hossain et al., 2015; Vinogradov and Holloway, 1999; Wang et al., 2016; York et al., 2010). The coupled chemo-mechanical behavior of viscoelastic polymers has also been studied in recent years. In the current literature on viscoelastic gels, one can find the experimental research by numerous groups (Chan et al., 2012; Keshavarz et al., 2017; Nam et al., 2016; Zhao et al., 2010). Further, continuum-level constitutive models for viscoelastic gels, which take into account the chemo-mechanical behavior have been developed (Chester, 2012; Hu and Suo, 2012). Nonetheless, the current state of the literature lacks sufficient quantity of data and observations to corroborate and calibrate the vast number of models.

It is also worth noting that recent years saw an extensive number of studies, both experimental and theoretical, involving poroelasticity (c.f., e.g., Galli et al., 2009; Hu and Suo, 2012; Hu et al., 2010; Wang and Hong, 2012). While these studies have provided an insight in the coupled diffusion-deformation behavior at smaller deformations, the response of polymeric gels undergoing large deformations is yet to be fully characterized and modeled.

The goal of this paper is to characterize the viscoelastic response of both dry and fully swollen polymeric gels through experimental observations and continuum level modeling. Towards our goal, we have developed an experimental procedure intended to capture the major aspects of the non-linear mechanical behavior of polymeric gels, including the viscoelastic response. To complement the experimental observations, we calibrate a constitutive model for viscoelastic polymeric gels. In what follows, we restrict our attention to the specific cases where the material is either completely dry, or fully swollen.

For our experiments we have chosen the commercially available material VHB 4910, since it is well known to exhibit viscoelastic behavior in the absence of fluid (Hossain et al., 2012; Wang et al., 2016). Also, we have observed that VHB 4910 swells when in contact with suitable solvents. Therefore, all of our experiments make use of n-Pentane, o-Xylene, and Toluene, as solvents in conjunction with VHB 4910 to create our polymeric gels. The continuum-level constitutive model is mechanically incompressible, includes viscoelasticity, and does not explicitly take diffusion into account. That is to say we consider time dependence in the mechanical response, however not in the diffusive response of the solvent, which is taken to be at a known and fixed degree of swelling.

The remainder of this paper is organized as follows, in Section 2 we overview some of the terminology and important details involved with mechanical testing of swollen polymeric gels. In Section 3 we present our experimental procedures, as well as analysis procedures for our measurements, and the corresponding results. In Section 4 we present the constitutive model used to interpret the experimental results and the model is calibrated in Section 5. Lastly, Section 6 provides some concluding remarks.

2. Preliminaries

It is worthwhile to make clear our assumptions used for mechanical testing of polymeric gels. First, for clarification, the nomenclature that will be used throughout is:

- *Virgin* — A dry sample, without any previous history of solvent exposure, or mechanical loading, is considered *virgin*.
- *Fully swollen* — A virgin sample, exposed to ample solvent, free of mechanical constraints, and allowed to swell until equilibrium, is considered *fully swollen*. This process is termed *free swelling*.

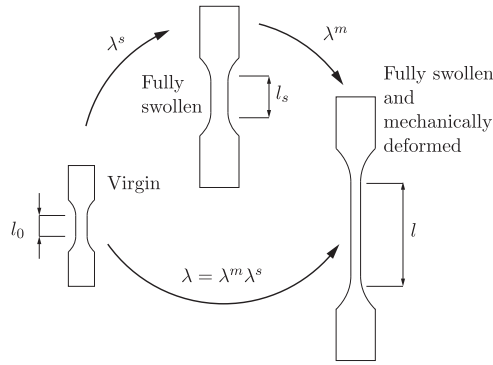


Fig. 1. Schematic of the multiplicative decomposition of the total uniaxial stretch into swelling and mechanical contributions.

- *Solvent cycled* – A virgin sample, first fully swollen, and then completely dried (deswollen), is considered *solvent cycled*. The process of swelling following by drying may be repeated numerous times. For example, a sample could be solvent cycled five times, that indicates a virgin sample was fully swollen and then freely dried five times.

When mechanically testing unswollen samples (either virgin or solvent cycled), in a uniaxial setting the total deformation that polymer network undergoes is the mechanical stretch λ^m . On the other hand, exposing that polymer network to an ample quantity of a suitable solvent for long enough time, in the absence of mechanical constraints or loading, will cause it to freely swell to equilibrium. The process of free swelling yields an isotropic volumetric expansion, and on a continuum level, a stress-free state – what we call fully swollen. The stretch caused by swelling is denoted by λ^s , assumed to be spherical, and when freely swollen λ^s is homogeneous inside a gel.¹ For our experiments on freely swollen gels, we consider the initial configuration for mechanical testing the freely swollen state, with a prior homogeneous swelling stretch λ^s . Uniaxial mechanical testing on the freely swollen polymer gels is achieved by displacement controlled deformation applied on the initially freely swollen material. This is shown schematically in Fig. 1. Further, as is common in the literature on the mechanics of gels, we employ a multiplicative decomposition of the total uniaxial stretch, making the total deformation of the swollen polymer gel

$$\lambda = \lambda^m \lambda^s. \tag{1}$$

Going further into the details, in reference with Fig. 1, the total uniaxial stretch is defined as

$$\lambda = \frac{l}{l_0} \tag{2}$$

where l is the deformed gauge length and l_0 is the virgin gauge length. The swelling stretch represents the ratio of the swollen length to virgin length

$$\lambda^s = \frac{l_s}{l_0}, \tag{3}$$

where l_s is the length of swollen material. Following Fig. 1 and (1), the mechanical stretch is the ratio of the mechanically deformed length to the freely swollen length, which can be written in the form

$$\lambda^m = \frac{l}{l_s} = \frac{l_s + u^m}{l_s} = 1 + \frac{u^m}{l_s}, \tag{4}$$

where u^m is the axial displacement caused by mechanical deformation. In the case of dry material without any swelling, we simply have $\lambda^s = 1$, and therefore $\lambda = \lambda^m$.

Since we are interested in assessing the rate-dependent behavior of polymeric gels, the rate of deformation is essential. To make the analysis as useful as possible, we use the mechanical stretch rate

$$\dot{\lambda}^m = \frac{\dot{u}^m}{l_s}, \tag{5}$$

and the total stretch rate at a fixed amount of swelling

$$\dot{\lambda} = \frac{\dot{u}^m}{l_0} = \dot{\lambda}^m \lambda^s. \tag{6}$$

The standard nominal (1st Piola) stress in uniaxial tension for dry material is given by

$$P = \frac{F}{A_0} \tag{7}$$

¹ In general, in the presence of mechanical or chemical constraints, λ^s need not be homogeneous inside a polymeric gel.

where F is the force signal obtained by the load cell, and A_0 is the dry nominal cross sectional area. Care must be taken in the choice of a stress measure used for fully swollen uniaxial tests. Prior to any mechanical loading, since the sample is fully swollen, but mechanically undeformed we have $\lambda^m = 1$ and $\lambda^s > 1$, leading to an initial stretch $\lambda = \lambda^s > 1$ prior to the application of any prescribed mechanical deformation. Therefore, we will also report on the stress measured per freely swollen cross sectional area, a mechanical Piola stress. Here the mechanical Piola stress is denoted by

$$P^m = \frac{F}{A^s}, \quad (8)$$

where A^s is the nominal cross sectional area of the fully swollen sample. Additionally, the Cauchy stress, or true stress, is the force per unit current cross sectional area. However since we are unable to measure the current cross sectional area during a test, and do not want to make unnecessary assumptions, we do not report it in this work.

Lastly, we will make frequent use of the stiffness in our analysis, which experimentally is taken simply as the slope of the uniaxial tension stress - stretch curve, measured at a specific deformation since it is not constant. Since our experiments are designed to obtain the material response at a fixed degree of swelling, we assume λ^s is a constant, therefore,

$$\frac{d(\bullet)}{d\lambda} = \frac{d(\bullet)}{d\lambda^m} \frac{d\lambda^m}{d\lambda} = \frac{d(\bullet)}{d\lambda^m} (\lambda^s)^{-1}. \quad (9)$$

Accordingly, we only report on stiffnesses measured relative to mechanical deformation in this work. Further, since the effective stiffness is what one would measure in the current deformed configuration, for dry and swollen samples the effective stiffness is

$$\frac{dP}{d\lambda^m}, \quad \text{and} \quad \frac{dP^m}{d\lambda^m}, \quad (10)$$

respectively. To experimentally measure the stiffness based on experimental data, we determine the slope of the stretch-stress curve at a specified stretch by fitting a line to five data points centered around the specified stretch.

3. Experimental procedures and results

In this section we report our experimental procedures for capturing the non-linear viscoelastic behavior of virgin, fully swollen, and solvent cycled polymeric materials, as well as the corresponding results. Our experiments are performed on the popular and widely known commercially available acrylic polymer VHB 4910. This material is chosen since virgin VHB is well known to exhibit highly viscoelastic non-linear behavior (Hossain et al., 2012; Wang et al., 2016).

The overall experimental scheme broadly consists of the following:

1. Uniaxial tension, stress relaxation, and creep testing on virgin samples;
2. Free swelling of virgin samples;
3. Uniaxial tension and stress relaxation on fully swollen samples;
4. Uniaxial tension and stress relaxation, on solvent cycled samples;

with more detail in what follows.

We commence the experimental procedure by determining the virgin baseline behavior of the polymer. To investigate the *time-independent* behavior of the virgin polymer, we perform a set of large deformation tensile tests, including load and unload, at a very slow mechanical stretch rate, accompanied by large deformation creep and stress relaxation testing. Next, to probe the *time-dependent* behavior of the virgin polymer we perform a set of tensile tests consisting of loading followed by unloading at various prescribed mechanical stretch rates. Further, to thoroughly probe the relaxation behavior of the virgin polymer, we perform a set of stress relaxation tests at a moderate prescribed stretch. After the uniaxial baseline data for the virgin polymer is obtained, we next move onto free swelling. To determine the swelling stretch caused by free swelling, VHB 4910 was immersed in three different solvents, n-Pentane, o-Xylene and Toluene, until equilibrium was reached, over 24 h. The next step involves repeating some of the uniaxial tests mentioned before, but now on fully swollen samples. The procedure consists of a similar set of uniaxial tests as used for the dry virgin material, to investigate the time-independent, time-dependent, and relaxation behavior of fully swollen VHB 4910. Lastly, virgin samples are freely swollen, followed by free drying of those same samples – what we have termed solvent cycled. Then, another similar set of uniaxial tests are performed again to determine if there is any measurable irreversible change to the mechanical behavior due to solvent cycling.

3.1. Experimental setup

All tensile tests reported here are conducted on an MTS Criterion Model 43 uniaxial testing machine at a fixed room temperature of 24 °C. We use dog-bone shaped specimens, and virgin samples are cut out from a roll of VHB 4910 tape using an ASTM D638-V cutting die. The nominal length, width, and thickness of the virgin gauge section are 9.49 mm, 3.18 mm, and 1 mm respectively. Importantly, since there are minute variations in the material, both thickness and width are measured prior to the start of all experiments. When dealing with very soft materials, the use of calipers or a micrometer can lead to false measurements due to the deformation of the material under the caliper jaws or micrometer anvils. Therefore, we use

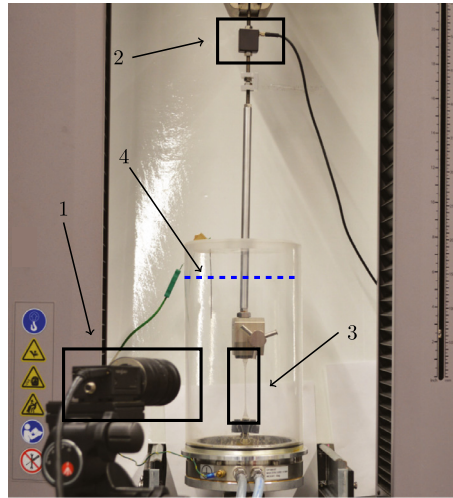


Fig. 2. Experimental setup for mechanical testing of a sample inside a fluid bath. Here, 1 denotes the digital camera, 2 the (5 pound) load cell, 3 an extended fully swollen gel sample, and 4 the water level.

a non-contact measurement based on photos of dry and swollen specimens, and use ImageJ (Rasband, 1997–2018) software to measure the thickness and the width of gauge section. Our experience shows that this leads to the best dimensionally repeatable data we were able to obtain. All the photos used for dimensional measurements reported here were taken with a Nikon-D3200 camera mounted on a tripod for repeatability.

To measure the deformation in our tensile experiments, the non-contact Digital Image Correlation (DIC) software Vic2D (Correlated Solutions) is employed and integrated with a digital camera (PointGrey GRAS-50S5M-C). Due to compliance of the testing machine, slippage, or other factors, post-processing DIC measurements of the gauge section have been found the most reliable method to obtain deformation data in these soft materials. Additionally, our DIC data acquisition system allows for concurrent image capture and force signal measurement. Since VHB is transparent, for virgin and solvent cycled samples, a number of black lines are applied to the gauge section with a permanent marker prior to testing to obtain color contrast for DIC measurements. However, the permanent marker was unreliable when applied to the surface of the fully swollen (wet) sample. Therefore, we applied fine black powder particles (silicon carbide grit, size 60) to the wet sample surface and they provide contrast for DIC.

To measure the force, a combination of a 5 pound load cell (Transducer Techniques MDB-5) and 100 g load cell (Transducer Techniques GSO-100) are used depending on the expected load encountered. The choice is made to obtain the best signal-to-noise ratio for each particular experiment. For example, a dry virgin material at very large stretch requires the 5 lb load cell, however a fully swollen load-unload tension test to moderate stretch will not exceed 100 g, and therefore the smaller load cell is used.

When left in air for 10 minutes, samples fully swollen with solvent (n-Pentane, o-Xylene, or Toluene) on average lost 20.7% of their mass through evaporation, compared to just 7.1% when completely submerged in water. Therefore, to mitigate the evaporation of solvent from the swollen gel, the tensile tests on fully swollen gels are performed inside a fluid bath filled with water, that is mounted in the load train of the testing machine, as shown in Fig. 2. We have found that immersion of the swollen gel in water significantly reduces the evaporation of the imbibed solvent, and is our best effort to ensure the solvent concentration is homogeneous inside the material.

In addition, the typical order of magnitude for solvent diffusivity in a polymeric gel is approximately 10^{-10} m²/s (c.f., e.g. Davis, 1974; Hayamizu et al., 1998), for a length scale of 1 mm, we estimate the characteristic diffusion time of about 2.75 h. Since the majority of our experiments take place on a much shorter timescale, when analyzing the experimental data we assume the solvent concentration is constant and uniform throughout for all of our mechanical tests.

It is important to note that, although the curvature of the fluid bath, along with the presence of water, somewhat distorts the images used for DIC in the transverse direction, it is not significant in the loading direction. A verification procedure is provided in the Appendix showing that the DIC measurements are acceptable with only minor error in this fluid bath setup. Therefore, we freely use DIC to measure the axial extension in our uniaxial experiments on submerged specimens.

Further, when performing a mechanical test on a sample submerged in a fluid bath, as in Fig. 2, the data recorded by the load cell is affected by buoyancy. To ensure the best quality force data, we include the buoyancy of the submerged grip, load train, and sample, when processing the experimental results. To determine the affect of buoyancy, we hold a swollen sample inside the top grip, and directly measure the change in force at different submerged depths. The recorded force per depth (N/m) is used when analyzing the data, allowing for the inclusion of buoyancy in the analysis. Details of the buoyancy calibration are provided in the Appendix.

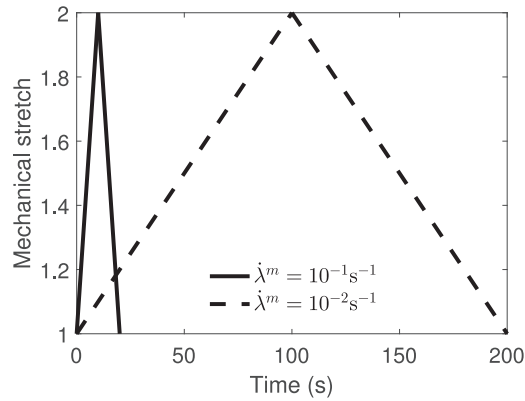


Fig. 3. Prescribed loading-unloading stretch profile to a maximum mechanical stretch of $\lambda^m = 2$.

3.2. Virgin uniaxial testing procedure

First, the dimensions of the gauge section width and thickness of each sample are measured using ImageJ (Rasband, 1997–2018) as described previously. The quasi-static large deformation tensile tests are performed at a constant stretch rate of $\dot{\lambda} = \dot{\lambda}^m = 10^{-4} \text{ s}^{-1}$, based on the virgin gauge section dimensions. The crosshead displacement is prescribed to obtain a maximum stretch of $\lambda = \lambda^m = 10$ based on the virgin gauge length, followed by unloading to the initial stretch of $\lambda = 1$ to probe the large deformation behavior and hysteresis in the material response. Later, DIC analysis is performed as a post-processing step to obtain the actual deformation in the gauge section.

For load-unload tensile tests at moderate stretch rates, we prescribe the crosshead displacement to obtain a maximum stretch of $\lambda = \lambda^m = 2$, and the unloading displacement to return to the initial stretch of $\lambda = \lambda^m = 1$ at a constant stretch rate. To assess rate dependency, two different rates are used $\dot{\lambda} = \dot{\lambda}^m = 10^{-2} \text{ s}^{-1}$ and 10^{-1} s^{-1} , with the prescribed loading profiles shown in Fig. 3.

Next, we perform a set of stress relaxation experiments. First, samples are loaded to a stretch $\lambda = \lambda^m = 2$, at a stretch rate of $\dot{\lambda} = \dot{\lambda}^m = 2 \times 10^{-1} \text{ s}^{-1}$, the fastest our screw driven testing machine can reliably move. After reaching the prescribed stretch, samples are then held at that fixed stretch for 1 h, while the force is being recorded to determine the stress relaxation. As usual, DIC analysis is performed as a post-processing step, used here to obtain the actual stretch in the gauge section during the relaxation experiment.

Lastly, to complement the quasi-static large deformation testing and to ensure a time-independent response of the virgin material, we additionally performed: (i) Stress relaxation testing at various stretch levels, until stress equilibrium has been reached over 24 h; and (ii) creep testing at various constant stresses, until stretch equilibrium has been reached over 24 h.

3.3. Free swelling procedure

The free swelling procedure commences by taking the photos of virgin samples for dimensional measurements. Then, the virgin samples are fully submerged in ample solvent inside sealed glass jars. The sealed jars are placed inside a fume hood, and the samples are allowed to undergo free swelling for over 24 h. During that time, the swelling process reaches equilibrium and samples are considered fully swollen. To ensure that equilibrium was reached, the mass of the samples is measured periodically using a Sartorius Practum213-1S scale.

To obtain the swelling stretch of the fully swollen samples, photos of fully swollen samples were taken. ImageJ (Rasband, 1997–2018) software is then used to measure the virgin and the fully swollen lengths, and the swelling stretch is obtained using (3). Assuming spherical swelling, the fully swollen sample dimensions are obtained by scaling the virgin dimensions by the swelling stretch. Therefore, the cross sectional area of the fully swollen gauge section is

$$A^s = (\lambda^s t_0)(\lambda^s w_0) = (\lambda^s)^2 A_0. \quad (11)$$

3.4. Fully swollen uniaxial testing procedure

Other than the samples being submerged in the water bath, the uniaxial testing procedure for a fully swollen gel is essentially the same as the dry procedure described in Section 3.2. The main differences lie in the care needed in analysis to account for the prior swelling deformation, and the affects of the water bath such as buoyancy. As before, DIC is used in all cases as a post processing step to assess the actual deformation in the gauge section.

Large deformation quasi-static tensile tests are performed at a very slow mechanical stretch rate of $\dot{\lambda}^m = 10^{-4} \text{ s}^{-1}$, based on the swollen length of the gauge section. Fully swollen samples were subjected to a prescribed total stretch of either $\lambda = 10$, or just prior to failure, followed by unloading to the initial stretch of $\lambda = \lambda^s$, which is the freely swollen stretch.

For moderate rate loading-unloading tensile tests, the sample is loaded to a mechanical stretch of $\lambda^m = 2$, which corresponds to a total stretch $\lambda = \lambda^m \lambda^s = 2\lambda^s$, followed by unloading to $\lambda^m = 1$, which matches the initial freely swollen total stretch of $\lambda = \lambda^s$. To assess rate dependency, two different rates are used $\dot{\lambda}^m = 10^{-2} \text{ s}^{-1}$ and 10^{-1} s^{-1} , and Fig. 3 shows the prescribed stretch profiles.

Finally, we perform a set of stress relaxation tests, in which the samples are first loaded to $\lambda^m = 2$ at a stretch rate $\dot{\lambda}^m = 2 \times 10^{-1} \text{ s}^{-1}$, and held at that fixed stretch for 1 h, while the force is being recorded to determine the stress relaxation behavior.

3.5. Solvent cycling procedure

As mentioned earlier, solvent cycling is the process of swelling, followed by drying. Following the free swelling procedure, some specimens were then allowed to freely dry. The free swelling procedure was already described in Section 3.3, and is followed again for solvent cycling. The free drying procedure is very similar, however the swollen samples are set inside a petri dish, free of constraint, in a fume hood for 48 h. Mass measurements are taken frequently along the process as described previously. We consider the sample to be completely dry once its mass is nearly equal (i.e., the same value relative to the instrument precision) to that of the dry virgin sample, implying all the solvent has evaporated from the polymer network.

3.6. Uniaxial testing procedure after solvent cycling

The uniaxial testing procedure of samples that underwent solvent cycling consists of nearly the identical set of experiments used to test virgin samples. First, the large deformation quasi-static response of the material is probed through uniaxial tensile tests at a very slow mechanical stretch rate of $\dot{\lambda}^m = 10^{-4} \text{ s}^{-1}$, based on the solvent cycled gauge section length (which coincides with the virgin length). For this purpose, the samples have been deformed to a prescribed mechanical stretch $\lambda^m = 10$. Next, to determine the hysteresis in the material response, along with the rate-dependence, we perform a set of load-unload tensile tests to a mechanical stretch of $\lambda^m = 2$, employing two different deformation rates $\dot{\lambda}^m = 10^{-2} \text{ s}^{-1}$ and 10^{-1} s^{-1} . Lastly, a set of stress relaxation tests at a fixed stretch of $\lambda^m = 2$ were performed with a relaxation time of over 1 h.

3.7. Experimental results

3.7.1. Uniaxial results on virgin specimens

The results of our uniaxial tests on virgin specimens are shown in Fig. 4. Specifically, Fig. 4a very clearly shows the large deformation response under very slow loading. Here, clear evidence of the chain-locking behavior of VHB 4910 is observed at a uniaxial mechanical stretch of $\lambda^m \approx 9$. Further, the dry virgin material exhibits pronounced rate-dependent behavior, which is observed in Figs. 4a and 4b. The load-unload tensile tests at two moderate rates show clear rate-dependence as well as significant hysteresis upon unloading due to viscoelastic effects. Fig. 4c shows the measured stress relaxation behavior at an applied stretch of $\lambda = 2$. From this figure one clearly observes relaxation, going from a nominal stress of just over 110 kPa and relaxing to just over 40 kPa over 1 h. In Fig. 4d the large deformation quasi-static tension test results at a rate of 10^{-4} s^{-1} are plotted along with the long term creep and relaxation data at equilibrium. Since the large deformation quasi-static tensile response has some hysteresis, we interpolated the creep and relaxation data (utilizing the smooth function in MATLAB) to obtain the time-independent response of the material.

To quantify the experimental observations and rate-dependent behavior of the material, we measure the stiffness and hysteresis at different stretch rates. The initial stiffness $\frac{dP}{d\lambda^m}$ is measured for all three $\dot{\lambda}^m$ employed in tensile testing. Additionally, from the data obtained using a large deformation quasi-static test, we also measure the stiffness near the maximum measurable, and midway. The amount of hysteresis is determined by the area enclosed by the loading and unloading path on the stress-stretch curve.

The measured effects of locking are clear, with an increase in stiffness $\frac{dP}{d\lambda^m}$ from 17.19 kPa at a stretch of 4.5 to 102.53 kPa at a stretch of 8.36. Further, the experimental results showcase a noticeable increase in initial stiffness with an increase in $\dot{\lambda}^m$, ranging from 60.2 kPa for the $\dot{\lambda}^m = 10^{-4} \text{ s}^{-1}$, 170.18 kPa for the $\dot{\lambda}^m = 10^{-2} \text{ s}^{-1}$, to 333.31 kPa for the $\dot{\lambda}^m = 10^{-1} \text{ s}^{-1}$. In addition to the increase in stiffness, one can notice an increase in hysteresis from 15.82 kPa at $\dot{\lambda}^m = 10^{-2} \text{ s}^{-1}$ to 31.41 kPa at $\dot{\lambda}^m = 10^{-1} \text{ s}^{-1}$.

We note that the tabulated data and comparisons to the fully swollen material is provided later in Section 3.7.3 when the fully swollen results are discussed.

3.7.2. Free swelling results

As mentioned previously, optical measurements of specimens before and after free swelling of VHB 4910 in various solvents provide a reliable measurement of the swelling stretch at equilibrium without constraints. Fig. 5 shows the virgin dry specimen, and the corresponding fully swollen specimen for the solvents: a) n-Pentane; b) o-Xylene; and c) Toluene. The average mass of our virgin samples is 0.495 g prior to solvent exposure. Our measurements show that a VHB 4910 specimen

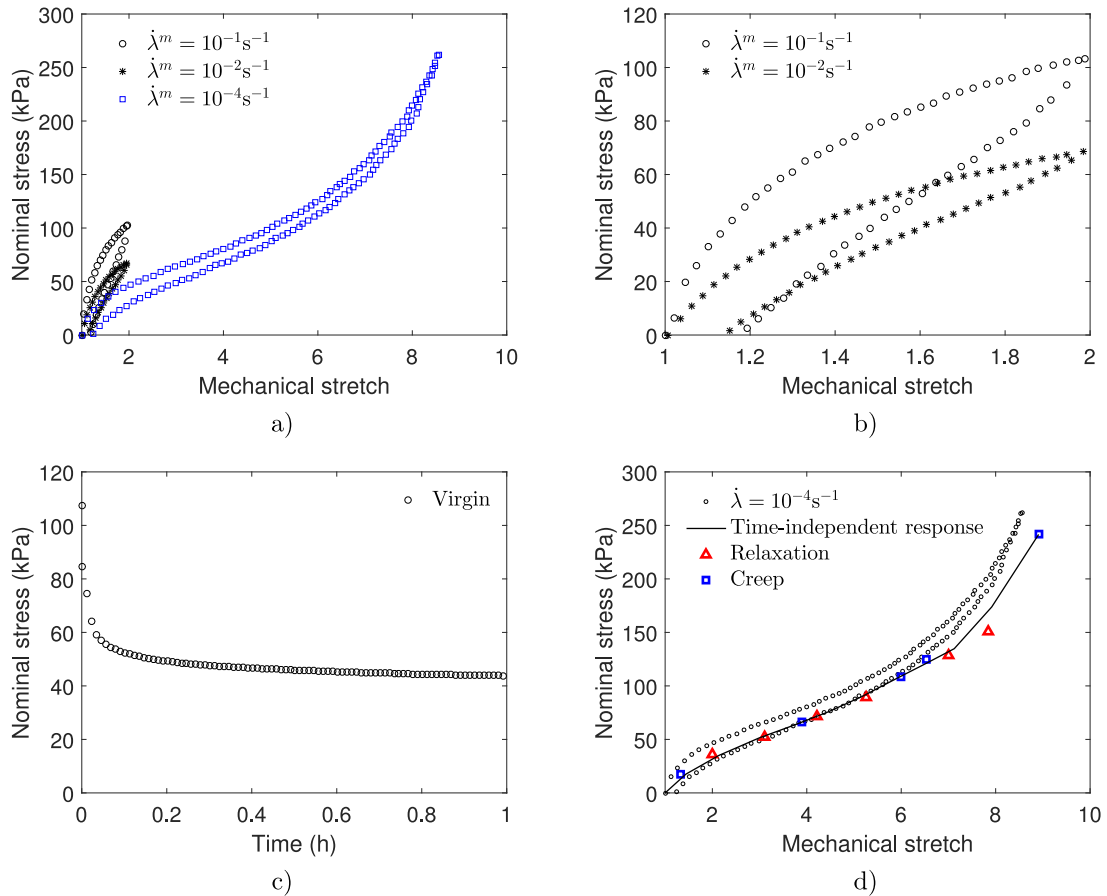


Fig. 4. Uniaxial experimental results for dry virgin specimens. a) Large deformation quasi-static and moderate rate load-unload uniaxial tensile tests, with nominal stress as a function of mechanical stretch λ^m , which in case of dry samples is the same as the total stretch λ . b) The same load-unload data at moderate rates in a smaller range of stretch for clarity. c) Stress relaxation for an applied mechanical stretch of 2. And d) comparison between the quasi-static large deformation tensile test and the time-independent behavior obtained through combination of stress relaxation and creep testing.

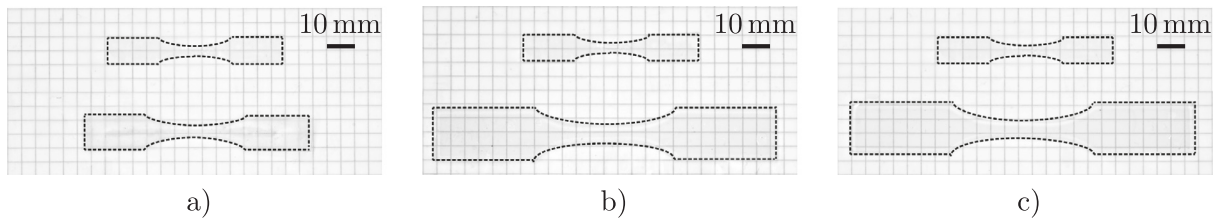


Fig. 5. VHB 4910 ASTM D638-V dog-bone specimens before and after free swelling to equilibrium, and also used for uniaxial testing. a) Dry and swollen with n-Pentane, with equilibrium swelling stretch $\lambda^s = 1.49$. b) Dry and swollen with o-Xylene with equilibrium swelling stretch $\lambda^s = 1.95$. c) Dry and swollen with Toluene with equilibrium swelling stretch $\lambda^s = 1.98$. We note that the dotted lines are drawn along the edges of specimens to emphasize the specimen boundary for this transparent material.

fully swollen in n-Pentane on average absorbs 0.66 g of solvent and has a swelling stretch of $\lambda^s = 1.49$. Similar measurements for o-Xylene show that it absorbs 3.47 g of solvent and has a swelling stretch of $\lambda^s = 1.95$. And lastly for Toluene, 3.40 g are absorbed and the swelling stretch is $\lambda^s = 1.98$. To ensure the equilibrium, the mass is measured periodically over 48 h. Fig. 6 clearly shows the swelling process reaching equilibrium in about 24 h, for all three solvents.

3.7.3. Uniaxial results on fully swollen specimens

The results of our uniaxial tests of fully swollen specimens are shown in Fig. 7 for tension tests on VHB fully swollen with n-Pentane, Fig. 8 for tension tests on VHB fully swollen with o-Xylene, Fig. 9 for tension tests on VHB fully swollen with Toluene, and Fig. 10 for relaxation tests on specimens fully swollen with all three solvents.

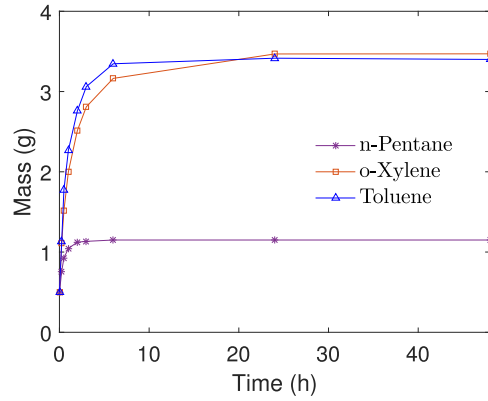


Fig. 6. Sample mass measured periodically over 48 h of free swelling indicating equilibrium is reached at 24 h.

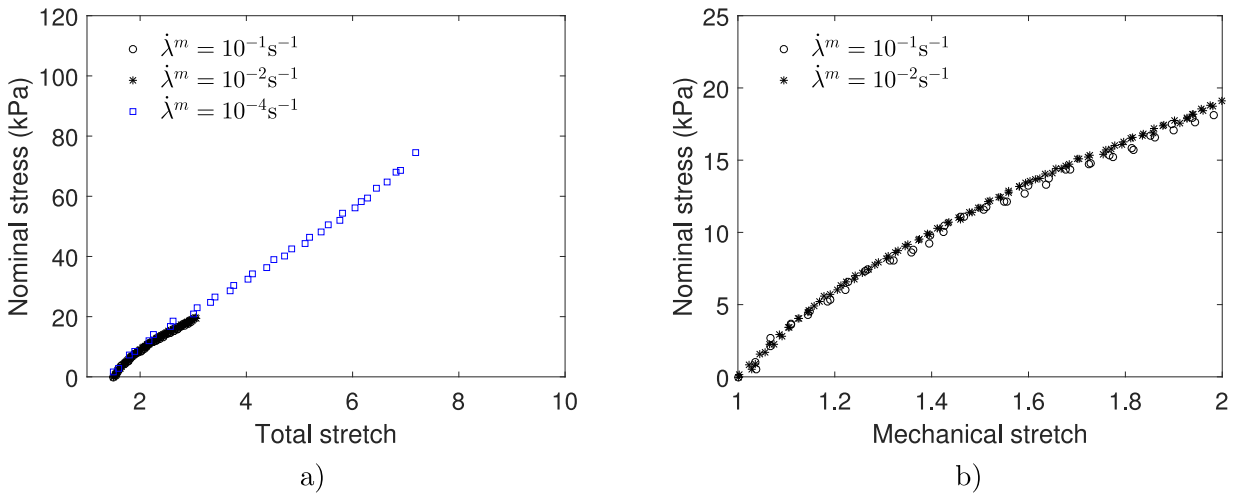


Fig. 7. Experimental results for samples swollen in n-Pentane. a) Large deformation quasi-static load-unload, along with load-unload moderate rate tests to $\dot{\lambda}^m = 2$, with results presented as a function of total stretch $\lambda = 1.49\lambda^m$. b) Load-unload tests to $\lambda^m = 2$ at moderate stretch rates and presented as a function of mechanical stretch.

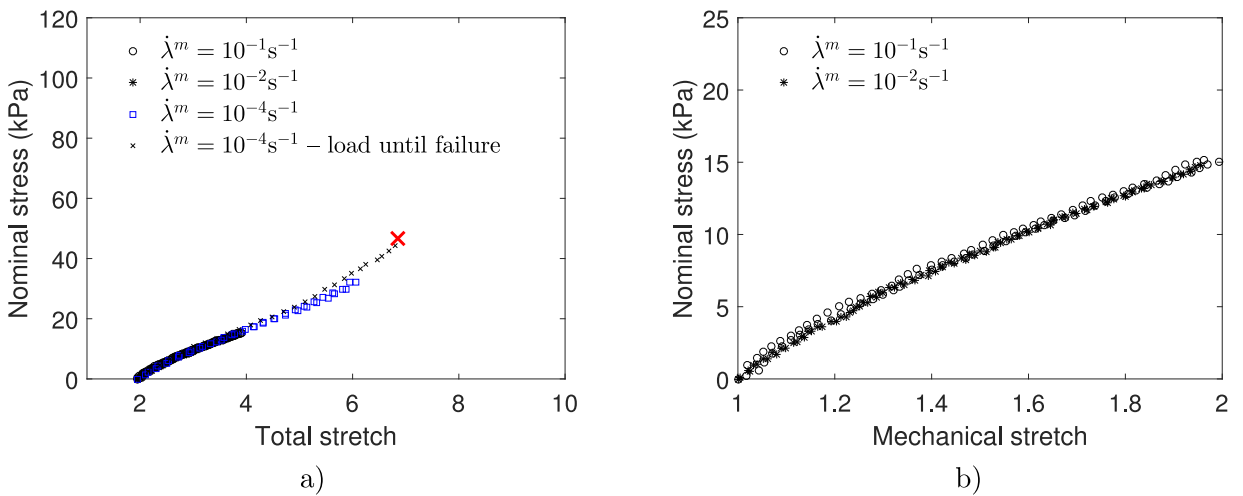


Fig. 8. Experimental results for samples swollen in o-Xylene. a) Large deformation, along with load-unload testing to $\lambda^m = 2$, with results as a function of total stretch $\lambda = 1.95\lambda^m$. b) Load-unload tests to $\lambda^m = 2$ at different mechanical stretch rates and presented as a function of mechanical stretch. The red \times indicates failure of the sample. (For interpretation of the references to colour in this figure legend, the reader is referred to the web version of this article.)

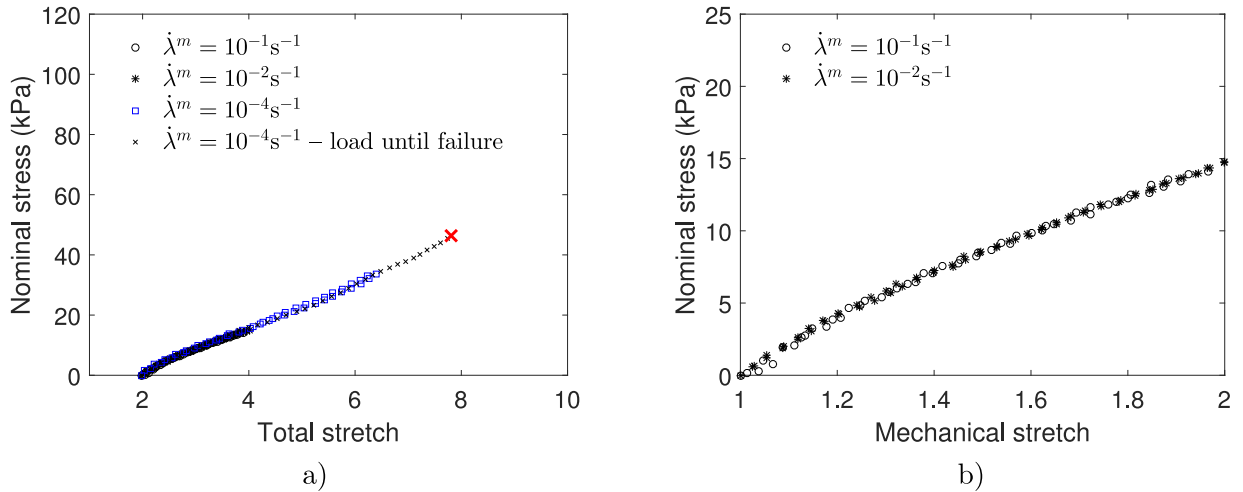


Fig. 9. Experimental results for samples swollen in Toluene. a) Large deformation, along with load-unload testing to $\lambda^m = 2$, with results as a function of total stretch $\lambda = 1.98\lambda^m$. b) Load-unload tests to $\lambda^m = 2$ at different mechanical stretch rates and presented as a function of mechanical stretch. The red \times indicates failure of the sample. (For interpretation of the references to colour in this figure legend, the reader is referred to the web version of this article.)

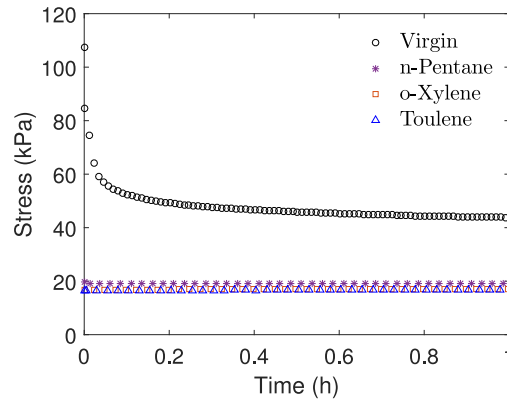


Fig. 10. Virgin and fully swollen stress relaxation results. The virgin experiment is plotted using the stress measure P , while the swollen experiments are plotted using the stress measure P^m .

First considering the tensile behavior of VHB 4910 fully swollen in n-Pentane, Fig. 7 shows the large deformation quasi-static load-unload response, as well as the load-unload response at a few fixed, but different, moderate stretch rates. Based on the large deformation tensile test we can observe no hysteresis in the response of the material, along with a decrease in the initial effective stiffness from 60.2 kPa to 27.53 kPa, as seen in Table 1. Also, we find that the material does not show any clear locking behavior when compared to the virgin material, with the stiffness increasing from 14.41 kPa at a total stretch of 4.5 to just 17.85 kPa at a stretch of 7.73, as shown in Table 2. Looking at the moderate rate load-unload data to a stretch of 2, the measured initial effective stiffness $\frac{dP^m}{d\lambda^m}$ drops to 32.74 kPa at $\dot{\lambda}^m = 10^{-2} \text{s}^{-1}$ and 34.29 kPa at $\dot{\lambda}^m = 10^{-1} \text{s}^{-1}$. The difference in stiffness at various stretch rates is negligible compared to the virgin material (see Table 1), and the samples exhibit an almost complete absence of rate-dependency in the response. Along with the decrease in stiffness,

Table 1
Measured initial effective stiffness, $\frac{dP}{d\lambda^m}$ for virgin, and $\frac{dP^m}{d\lambda^m}$ for fully swollen samples at different applied stretch rates.

$\dot{\lambda}^m$ (s^{-1})	10^{-4}	10^{-2}	10^{-1}
Virgin (kPa)	60.20	170.18	333.31
n-Pentane (kPa)	27.53	32.74	34.29
o-Xylene (kPa)	24.73	23.94	26.59
Toluene (kPa)	21.58	22.01	21.44

Table 2

Chain-locking behavior observed through stiffness measurements on virgin ($\frac{dP^m}{d\lambda^m}$) and fully swollen ($\frac{dP^m}{d\lambda^m}$) samples with data taken at a stretch rate of $\dot{\lambda} = 10^{-4} \text{s}^{-1}$. For samples swollen with o-Xylene and Toluene, we take the maximum λ to be at the failure.

	Initial Stiffness (kPa)	Stiffness at $\lambda = 4.5$ (kPa)	Stiffness near max. λ (kPa)
Virgin	60.20	17.19	102.53 at ($\lambda = 8.36$)
n-Pentane	27.53	14.41	17.85 at ($\lambda = 7.73$)
o-Xylene	24.73	19.36	24.75 at ($\lambda = 6.85$)
Toluene	21.58	13.16	18.49 at ($\lambda = 7.81$)

Table 3

Measured hysteresis for a maximum mechanical stretch of 2 for virgin and fully swollen samples at different applied stretch rates.

$\dot{\lambda}^m$ (s^{-1})	10^{-2}	10^{-1}
Virgin (kPa)	15.82	31.41
n-Pentane (kPa)	0.37	0.84
o-Xylene (kPa)	0.18	0.46
Toluene (kPa)	0.6	0.33

one can observe the lack of hysteresis, with the measured hysteresis area going from 15.82 kPa to 0.37 kPa at $\dot{\lambda}^m = 10^{-2} \text{s}^{-1}$, and from 31.41 kPa to 0.84 kPa at $\dot{\lambda}^m = 10^{-1} \text{s}^{-1}$, as seen in Table 3. *In summary, the load-unload tensile experiments at various rates show no signs of rate-dependence or hysteresis.*

Next, considering the tensile behavior of VHB 4910 fully swollen in o-Xylene, Fig. 8 shows the large deformation quasi-static load-unload response, as well as the load-unload response at a few fixed, but different, moderate stretch rates. Based on the large deformation tensile test we can observe the absence of hysteresis in the material response, followed by the decrease in the initial effective stiffness from 60.2 kPa to 24.73 kPa, as seen in Table 1. Also, we find that the material has failed at a total stretch of 6.85, whereas the virgin material was still intact. Further, the material does not show any clear locking behavior compared to the virgin material, with an increase in stiffness from 19.36 kPa at a total stretch of 4.5, to 24.75 kPa at the failure stretch, as seen in Table 2. Measuring the initial effective stiffness $\frac{dP^m}{d\lambda^m}$ for moderate rate load-unload results, we notice the drop to 23.94 kPa at $\dot{\lambda}^m = 10^{-2} \text{s}^{-1}$ and 26.59 kPa at $\dot{\lambda}^m = 10^{-1} \text{s}^{-1}$. The difference in stiffness at various stretch rates is negligible compared to the virgin material, displaying almost the complete absence of rate-dependency in the response, as seen in Table 1. Along with the decrease in stiffness, we measure almost a complete lack of hysteresis, with the measured hysteresis area going from 15.82 kPa to 0.18 kPa at $\dot{\lambda}^m = 10^{-2} \text{s}^{-1}$, and from 31.41 kPa to 0.46 kPa at $\dot{\lambda}^m = 10^{-1} \text{s}^{-1}$, as seen in Table 3. *Again, the load-unload tensile experiments at various rates show no apparent signs of rate-dependence or hysteresis.*

Further, considering the tensile behavior of VHB 4910 fully swollen in Toluene, Fig. 9 shows the large deformation quasi-static load-unload response, as well as the load-unload response at a few fixed, but different, moderate stretch rates. Based on the large deformation tensile test we can observe the lack of hysteresis in the material response, followed by the decreases in the initial effective stiffness from 60.2 kPa to 21.58 kPa, as seen in Table 1. Also, we find that the material has failed at a total stretch of 7.81, whereas the virgin material was still intact. The material does not show any clear locking behavior compared to the virgin material, with an increase in stiffness from 13.16 kPa at a total stretch of 4.5, to 18.49 kPa at the failure stretch, as shown in Table 2. Measuring the initial effective stiffness $\frac{dP^m}{d\lambda^m}$ from moderate rate load-unload data, we observe a drop to 22.01 kPa at $\dot{\lambda}^m = 10^{-2} \text{s}^{-1}$ and 21.44 kPa at $\dot{\lambda}^m = 10^{-1} \text{s}^{-1}$. The difference in stiffness at various stretch rates is negligible compared to the virgin material, displaying the absence of rate-dependency in the response, as observed in Table 1. Along with the decrease in stiffness, we notice the lack of hysteresis, with a decrease in the measured hysteresis area from 15.82 kPa to 0.6 kPa at $\dot{\lambda}^m = 10^{-2} \text{s}^{-1}$, and from 31.41 kPa to 0.33 kPa at $\dot{\lambda}^m = 10^{-1} \text{s}^{-1}$, as seen in Table 3. *Again, the load-unload tensile experiments at various rates show no signs of rate-dependence or hysteresis.*

Lastly, Fig. 10 shows the stress relaxation behavior of VHB 4910 fully swollen in all three solvents with the virgin data superimposed. After a rapid crosshead displacement, the mechanical stretch is held fixed at $\lambda^m = 2$ for 1 h. What is most notable about these results are that the behavior is nearly all elastic for all fully swollen gels. VHB 4910 swollen in o-Xylene and Toluene do not even have a measurable amount of stress relaxation, and the specimens fully swollen with n-Pentane show a dramatically decreased amount of relaxation, over a much shorter time span compared to the virgin case.

3.7.4. Uniaxial results on dry, solvent cycled specimens

Thus far, it is clear that the uptake of solvent has an affect on the mechanical behavior of these materials. To assess if swelling causes irreversible changes to the mechanical behavior, we solvent cycle – freely swell, then freely dry – and then use those samples for uniaxial tests. Mass measurements shown in Fig. 11 show all three solvents completely evaporating

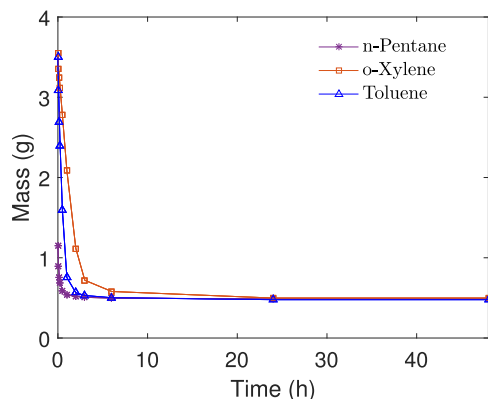


Fig. 11. Mass of initially fully swollen samples, measured periodically during 48 h of free drying.

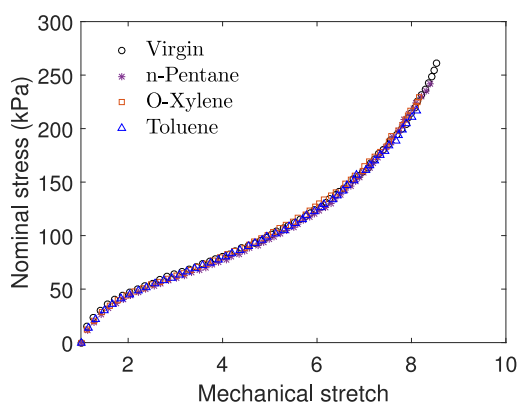


Fig. 12. Large deformation uniaxial tensile loading results after solvent cycling 5 times with n-Pentane, o-Xylene and Toluene, along with a virgin sample. The results lie almost completely on top of each other.

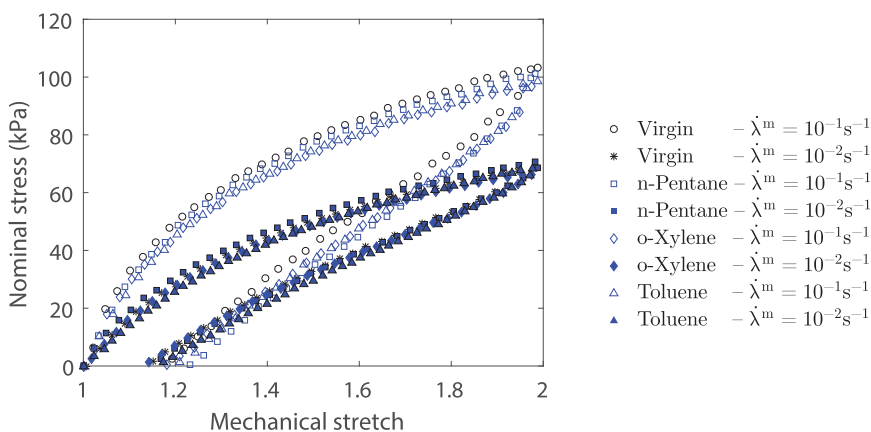


Fig. 13. Uniaxial load-unload tensile test results after solvent cycling 5 times with n-Pentane, o-Xylene and Toluene. For ease of comparison, we also show the virgin results.

after about 24 h of free drying, ensuring fully dried samples for mechanical testing. For samples that have been solvent cycled five times, Fig. 12 shows the reappearance of chain-locking behavior, and Fig. 13 shows the reappearance of the viscoelastic response for uniaxial load-unload experiments. Additionally, Fig. 14 shows a reappearance of viscoelasticity for the material subjected to a stress relaxation experiment. These combined results show that *prior solvent cycling has no significant residual effects on the overall response of the polymer, which we take as an indication of the reversibility of the process.*

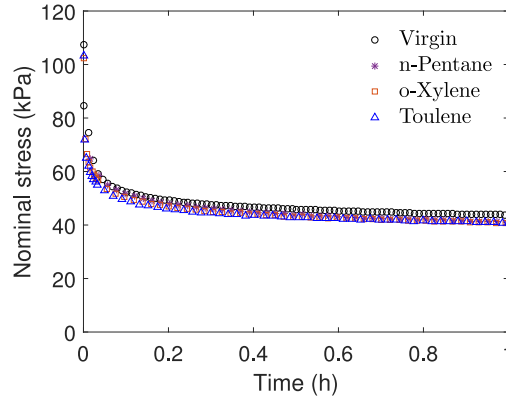


Fig. 14. Stress relaxation of virgin VHB, and after 5 cycles of swelling with n-Pentane, o-Xylene and Toluene. The results lie almost completely on top of each other.

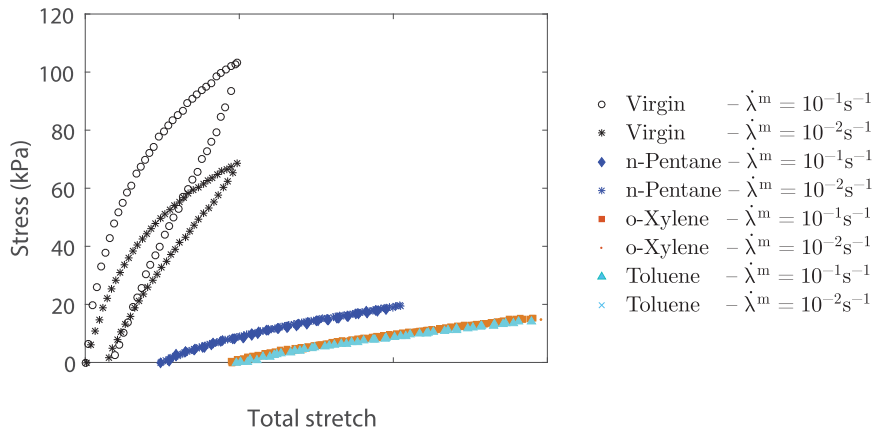


Fig. 15. A subset of the experimental results showing the load-unload response for moderate rates displaying the clear affect of swelling on the behavior. The virgin experiments are plotted using the stress measure P , while the swollen experiments are plotted using the stress measure P^m .

3.8. Summary of the experimental results

Fig. 15 shows already presented data, but now with multiple stretch-stress curves all superimposed atop each other, and immediately the change in behavior is visible. The behavior of virgin samples shows clear viscoelastic effects. However, the fully swollen results show no signs of rate dependency, nor hysteresis, with load-unload stretch-stress curves obtained at different rates being almost completely on top of each other. Measurements of the hysteresis, stiffness, and stress-stretch behavior all lead toward the hypothesis that the fully swollen material has lost nearly all viscoelasticity, and the fully swollen material behaves like a non-linear elastic material. Further, our solvent cycling results show that prior solvent cycling has no significant residual effects on the overall response of the polymer, which we take as an indication of the reversibility of the process.

Based on some discussions in the literature (e.g., Fetters et al., 1994; Urayama et al., 2001) one possible mechanism for this change in behavior is that when the polymer network is expanded by introducing solvent molecules, the interaction between polymer chains becomes very small because the distance of the individual chains becomes larger, resulting in the absence of viscosity.

Additionally, the well known and prevalent Flory and Rehner (1943b) model predicts the effective modulus under uniaxial tension to be $E = E_d J^{-1/3}$, where E_d is the dry elastic modulus (Okumura et al., 2016). However, based on the quasi-static results shown in Table 1 we find that the effective modulus is not a function of the swelling ratio alone and is affected by other factors such as the specific solvent. Here o-Xylene has an equilibrium swelling stretch of $\lambda^s = 1.95$ and Toluene has $\lambda^s = 1.98$, based on the Flory and Rehner (1943b) model we should expect the ratio of moduli to be

$$\frac{E_{\text{o-Xylene}}}{E_{\text{Toluene}}} = \frac{J_{\text{o-Xylene}}^{-1/3}}{J_{\text{Toluene}}^{-1/3}} = \frac{\lambda_{\text{Toluene}}^s}{\lambda_{\text{o-Xylene}}^s} = \frac{1.98}{1.95} = 1.015$$

however the measured ratio is 1.146, over a 10% difference.

4. Constitutive model

In this section we overview a continuum-level constitutive model for polymeric gels, which aims to give particular attention to the viscoelastic response. The large deformation time-independent response of the polymer is modeled employing a non-Gaussian statistical mechanics model, which takes into account the limited extensibility of polymer chains (Anand, 1996; Arruda and Boyce, 1993), as well as a scaling exponent on the swelling ratio to account for the change in effective stiffness (Okumura et al., 2016; Zamani and Pence, 2017). Viscous effects are modeled following the micromechanically motivated approach by Green and Tobolsky (1946) and Linder et al. (2011). Lastly, the mixing between the polymer network and solvent is accounted for by the Flory-Huggins model (Flory, 1942; Huggins, 1942). The model, in its current form, follows from the previous work of our research group (Chester, 2012; Chester and Anand, 2010; 2011; Chester et al., 2015) and is summarized in this section for clarity. However, in contrast to our previous models, we do not explicitly account for solvent diffusion, and only consider equilibrium conditions. This assumption is made since our experiments are not intended to probe the diffusive behavior of these polymeric gels. Lastly, while it is well known that more complete constitutive models exist to capture the elastic modulus of swollen elastomers (cf. e.g., Okumura et al., 2016), we do not burden ourselves with the extra complexity since the focus here is on the viscoelastic behavior.

4.1. Kinematics

The model is based on a multiplicative decomposition of the deformation gradient into mechanical and swelling parts

$$\mathbf{F} = \mathbf{F}^m \mathbf{F}^s \quad \text{with} \quad \mathbf{F}^s = \lambda^s \mathbf{1}, \quad \lambda^s \geq 1. \quad (12)$$

In (12) $\mathbf{F}^s(\mathbf{x}_R)$ represents the local distortion of the material due to swelling at an arbitrary material point \mathbf{x}_R of the undeformed body \mathcal{B}_R , and λ^s is the swelling stretch. This local deformation accounts for the swelling of the material due to absorbed solvent molecules. $\mathbf{F}^m(\mathbf{x}_R)$ represents the subsequent mechanical stretching and rotation of this coherent swollen network structure.

With respect to (12), the right and left Cauchy-Green tensors are

$$\mathbf{C} = \mathbf{F}^T \mathbf{F} = (\mathbf{F}^m \mathbf{F}^s)^T (\mathbf{F}^m \mathbf{F}^s) = \mathbf{F}^{mT} \mathbf{F}^m (\lambda^s)^2 = \mathbf{C}^m (\lambda^s)^2, \quad \text{and} \quad (13)$$

$$\mathbf{B} = \mathbf{F} \mathbf{F}^T = (\mathbf{F}^m \mathbf{F}^s) (\mathbf{F}^m \mathbf{F}^s)^T = \mathbf{F} \mathbf{F}^{mT} (\lambda^s)^2 = \mathbf{B}^m (\lambda^s)^2, \quad (14)$$

respectively.

Next, we assume that the mechanical response of the solvent and polymeric material is purely incompressible, and therefore $J^m = 1$. Further, we assume that the only volume change is due to swelling caused by the solvent, which is given by

$$J^s = 1 + \Omega c_R, \quad (15)$$

where Ω is the molar volume of the solvent and c_R is solvent concentration measured in moles of fluid absorbed per unit reference volume. In addition, since

$$J^s = \det \mathbf{F}^s = (\lambda^s)^3, \quad (16)$$

and with respect to (15), we may write

$$\lambda^s = (1 + \Omega c_R)^{1/3}. \quad (17)$$

4.2. Free energy

The experimental observations clearly show the material to be viscoelastic when dry, and also capable of undergoing swelling deformation in the presence of an ample solvent. To model the features of such a material, we consider the following three contributions to the free energy: (i) a time-independent contribution to account for the long time mechanical behavior; (ii) a time-dependent contribution to account for viscous effects; and (iii) a chemical mixing contribution to account for mixing between the solvent and polymer network. Thus, our basic form of the free energy function which accounts for the combined effects of mechanical stretching, swelling and mixing consists of three parts

$$\psi_R = \psi_R^{\text{TI}} + \sum_{\gamma} \psi_R^{\text{TD}(\gamma)} + \psi_R^{\text{chem}} \quad (18)$$

where ψ_R^{TI} models time-independent response, $\sum_{\gamma} \psi_R^{\text{TD}(\gamma)}$ models time-dependent behavior employing γ viscous mechanisms, and ψ_R^{chem} is the chemical free energy of mixing between the polymer network and the solvent.

For the time-independent free energy we adopt the statistical mechanics based Arruda-Boyce model (Anand, 1996; Arruda and Boyce, 1993) which takes into account the limited extensibility of polymer chains, coupled with a scaling exponent to account for stiffness changes (Okumura et al., 2016),

$$\psi_R^{\text{TI}} = G_0 \lambda_L^2 J^q \left[\left(\frac{\lambda}{\lambda_L} \right) \beta + \ln \left(\frac{\beta}{\sinh \beta} \right) - \left(\frac{1}{\lambda_L} \right) \beta_0 - \ln \left(\frac{\beta_0}{\sinh \beta_0} \right) - 3J^{2/3} \right] + G_0 \lambda_L^2 [3J^{2/3}] - G_0 \left(\frac{\lambda_L \beta_0}{3} \right) \ln J. \quad (19)$$

Here G_0 is the initial shear modulus, λ_L is the locking stretch, and $\bar{\lambda} = \sqrt{\text{tr}\mathbf{C}/3}$ is the effective stretch. Additionally, β and β_0 are functions given by

$$\beta = \mathcal{L}^{-1}\left(\frac{\bar{\lambda}}{\lambda_L}\right) \quad \text{and} \quad \beta_0 = \mathcal{L}^{-1}\left(\frac{1}{\lambda_L}\right), \tag{20}$$

where \mathcal{L}^{-1} is the inverse of the Langevin function, $\mathcal{L}(\bullet) = \text{coth}(\bullet) - 1/(\bullet)$. The locking stretch, λ_L , is the effective stretch where the polymer network is fully extended and cannot extend any further.

For the time-dependent contribution to the free energy, we follow the approach of Green and Tobolsky (1946) and Linder et al. (2011) which takes the form

$$\psi_R^{\text{TD}(\gamma)} = \frac{1}{2} G_{\text{TD}}^{(\gamma)} [(\mathbf{A}^{(\gamma)} : \mathbf{C}^m - 3) - \ln(\det \mathbf{A}^{(\gamma)})] \tag{21}$$

where $G_{\text{TD}}^{(\gamma)}$ are the shear moduli for each viscous mechanism γ . The evolution equation of each tensorial internal variable $\mathbf{A}^{(\gamma)}$ is given in the form

$$\dot{\mathbf{A}}^{(\gamma)} = \frac{1}{\tau^{(\gamma)}} ((\mathbf{C}^m)^{-1} - \mathbf{A}^{(\gamma)}), \quad \mathbf{A}(\mathbf{x}_R, t = 0) = \mathbf{1}, \tag{22}$$

where $\tau^{(\gamma)}$ is the relaxation time for each γ .

We adopt a Flory–Huggins (Flory, 1941; Huggins, 1942) model for the chemical mixing free energy which takes into account the mixing of polymer and solvent molecules

$$\psi_R^{\text{chem}} = \mu^0 c_R + R\vartheta c_R \left(\ln \left(\frac{\Omega c_R}{1 + \Omega c_R} \right) + \chi \left(\frac{1}{1 + \Omega c_R} \right) \right). \tag{23}$$

Where μ^0 is the chemical potential of the solvent, R is the universal gas constant, ϑ the absolute temperature, and χ polymer-solvent interaction parameter.

4.3. Cauchy stress

The Cauchy stress \mathbf{T} is given by

$$\mathbf{T} = J^{-1} \left(2\mathbf{F}^m \frac{\partial \psi_R}{\partial \mathbf{C}^m} \mathbf{F}^{mT} - p\mathbf{1} \right) = J^{-1} \left[GJ^q (\lambda^s)^2 \mathbf{B}^m + \sum_{\gamma} G_{\text{TD}}^{(\gamma)} \mathbf{F}^m \mathbf{A}^{(\gamma)} \mathbf{F}^{mT} - p^* \mathbf{1} \right], \tag{24}$$

where the shear modulus $G = G_0 \left(\frac{\lambda_L}{3\lambda}\right) \mathcal{L}^{-1}\left(\frac{\bar{\lambda}}{\lambda_L}\right)$ is a function of stretch, and p a scalar pressure field to satisfy the mechanical incompressibility constraint. The term p^* simply aggregates all of the spherical terms that arise.

4.4. Chemical potential

Based on the thermodynamic derivation found in the previous work from our group (c.f., e.g. Chester and Anand, 2010), and using the free energy form (18), the chemical potential μ is given by

$$\mu = \frac{\partial \psi_R}{\partial c_R} - \frac{1}{3} \text{tr} \mathbf{T} \Omega = \mu^0 + R\vartheta \left(\ln \left(\frac{\Omega c_R}{1 + \Omega c_R} \right) + \frac{1}{1 + \Omega c_R} + \chi \frac{1}{(1 + \Omega c_R)^2} \right) + (p - G_0) \frac{\Omega}{1 + \Omega c_R}. \tag{25}$$

Further, since we do not account for diffusion, the role of the chemical potential serves to obtain the conditions for chemical equilibrium, which is obtained when $\mu = \mu^0$. A few examples of when this may be put to use are to obtain the parameter χ in a free swelling experiment, or obtaining the swelling stretch for a given loading.

4.5. Specialized constitutive equations for uniaxial tension and free swelling/drying

When specialized for uniaxial tension, the constitutive model reduces to a one-dimensional set of equations, in which case the Cauchy stress takes the form

$$\sigma = \underbrace{J^{-1} GJ^q (\lambda^s)^2 \left[(\lambda^m)^2 - \frac{1}{\lambda^m} \right]}_{\text{Time-independent contribution}} + \underbrace{J^{-1} \sum_{\gamma} G_{\text{TD}}^{(\gamma)} \left[(\lambda^m)^2 A^{(\gamma)} - \frac{1}{\lambda^m \sqrt{A^{(\gamma)}}} \right]}_{\text{Time-dependent contribution}}, \tag{26}$$

where σ is the Cauchy stress in the loading direction. The evolution equation of each $A^{(\gamma)}$ in case of uniaxial tension is given in the form

$$\dot{A}^{(\gamma)} = \frac{1}{\tau^{(\gamma)}} ((\lambda^m)^{-2} - A^{(\gamma)}). \tag{27}$$

Further, with respect to (7) and (8) we obtain the uniaxial nominal stress per unit virgin cross sectional area

$$P = \underbrace{GJ^q \lambda^s \left[\lambda^m - \frac{1}{(\lambda^m)^2} \right]}_{\text{Time-independent contribution}} + \underbrace{\sum_{\gamma} G_{\text{TD}}^{(\gamma)} (\lambda^s)^{-1} \left[\lambda^m A^{(\gamma)} - \frac{1}{(\lambda^m)^2 \sqrt{A^{(\gamma)}}} \right]}_{\text{Time-dependent contribution}} \quad (28)$$

and the mechanical nominal stress per unit freely swollen cross sectional area

$$P^m = \underbrace{GJ^q (\lambda^s)^2 \left[\lambda^m - \frac{1}{(\lambda^m)^2} \right]}_{\text{Time-independent contribution}} + \underbrace{\sum_{\gamma} G_{\text{TD}}^{(\gamma)} \left[\lambda^m A^{(\gamma)} - \frac{1}{(\lambda^m)^2 \sqrt{A^{(\gamma)}}} \right]}_{\text{Time-dependent contribution}}, \quad (29)$$

respectively. For clarity, here we explicitly labeled the time-independent and time-dependent contributions to the materials behavior.

For mechanical testing and shape change measurements of all of our samples, we assume chemical equilibrium, and accordingly $\mu = \mu^0$. Therefore, following (25), we obtain

$$R\theta (\ln(1 - (\lambda^s)^{-3}) + (\lambda^s)^{-3} + \chi (\lambda^s)^{-6}) + (p - G_0) \Omega (\lambda^s)^{-3} = 0. \quad (30)$$

Which as mentioned before may be used to estimate χ in free swelling, or more generally the amount of solvent that a gel would uptake for a given loading condition.

5. Calibration

The constitutive model is calibrated in MATLAB for uniaxial conditions using the built-in least squares function `lsqnonlin`. The model calibration consists of multiple distinct steps that build upon each other. First, we determine the time-independent behavior of the virgin dry material in the absence of any solvent to obtain the time-independent material parameters G_0 and λ_L . Those time-independent material parameters are then held fixed for calibration of the time-dependent behavior for the dry virgin material in the absence of any solvent to obtain the time-dependent material parameters $G_{\text{TD}}^{(\gamma)}$ and $\tau^{(\gamma)}$, along with γ . Next, using free swelling data, the constitutive model is calibrated to obtain the polymer-solvent interaction parameter χ , for all of the polymer-solvent combinations in use in this paper implementing the previously calibrated equilibrium material parameters. Next, following the same procedure used for the virgin uniaxial tests, we calibrate our model to the experimental data obtained in our experiments on fully swollen samples. Lastly, also worth mentioning is that the calibration is performed separately for each of the solvents used.

5.1. Calibration of the time-independent behavior

5.1.1. Calibration of the virgin time-independent behavior

To determine the time-independent behavior of dry virgin VHB 4910, we calibrate our constitutive model against the time-independent data obtained through the combination of stress relaxation and creep testing, seen in Fig. 4d. Fig. 16a shows the calibrated constitutive model is in a good agreement with the experimental data on dry virgin material, and the calibrated material parameters G_0 and λ_L are provided in Table 4. We note that since the material is incompressible, and dry, the terms related to q will not affect the response and therefore q is not yet considered.

5.1.2. Calibration of the fully swollen time-independent behavior

Figs. 16b, 16c and 16d show the calibrated model along with the experimental data for samples fully swollen in n-Pentane, o-Xylene, and Toluene, respectively. For the samples swollen with o-Xylene and Toluene, we calibrated the model against the experimental data from large deformation tensile testing until failure. The initial shear modulus G_0 and locking stretch λ_L obtained from virgin calibration are held fixed, and the corresponding material parameter q obtained when fully swollen in each solvent is provided in Table 4.

Table 4
Calibrated time-independent material parameters.

	G_0 (kPa)	λ_L	q
Virgin	15.10	7.02	N/A
n-Pentane	15.10	7.02	-1.07
o-Xylene	15.10	7.02	-0.89
Toluene	15.10	7.02	-0.95

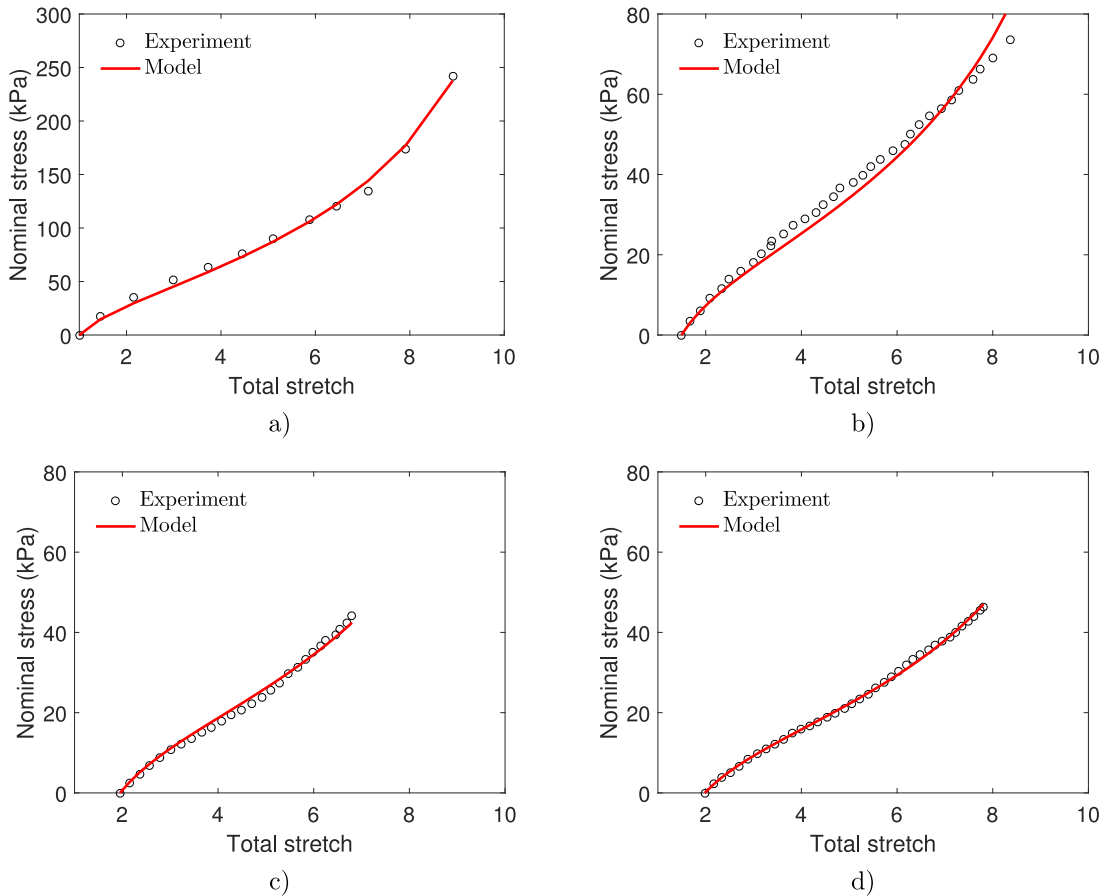


Fig. 16. Calibration of the time-independent behavior for VHB 4910 when (a) virgin, and and fully swollen with (b) n-Pentane, (c) o-Xylene and (d) Toluene. Here, G_0 and λ_L is obtained from virgin calibration and it's held constant throughout. The model is then calibrated for q against the fully swollen data.

5.2. Calibration of the time-dependent behavior

5.2.1. Calibration of the virgin time-dependent behavior

To calibrate the time-dependent portion of the constitutive model, we hold the virgin time-independent parameters fixed, and perform a least squares fit to the experimental data from load-unload tensile tests and stress relaxation tests on virgin samples. To keep the number of viscous mechanisms reasonably low, while still adequately modeling the behavior, we have found that three viscous mechanisms ($\gamma = 3$) are sufficient. Figs. 17a and 17b show the calibrated model along with the experimental data. Values for the time-dependent material parameters $G_{TD}^{(\gamma)}$ and $\tau^{(\gamma)}$ for virgin samples are presented in Table 5.

5.2.2. Calibration of the fully swollen time-dependent behavior

The comparison between the calibrated model and the loading-unloading experimental data for fully swollen samples is shown in Fig. 17c, e and g, and showcases the ability of our model to account for the lack of both energy dissipation and rate dependent behavior of fully swollen material. Further, calibration of the constitutive model against the stress relaxation data for fully swollen samples is in a good agreement with the experimental observation regarding the absence of stress

Table 5
Calibrated time-dependent material parameters.

	$G_{TD}^{(1)}$ (kPa)	$\tau^{(1)}$ (s)	$G_{TD}^{(2)}$ (kPa)	$\tau^{(2)}$ (s)	$G_{TD}^{(3)}$ (kPa)	$\tau^{(3)}$ (s)
Virgin	38.29	6.91	14.41	165.86	12.87	1.07×10^4
n-Pentane	0.33	0.26	0.08	1.57×10^3	1.31	9.99×10^3
o-Xylene	0.00	0.00	0.00	0.00	0.00	0.00
Toluene	0.47	0.00	0.00	0.00	0.00	0.00

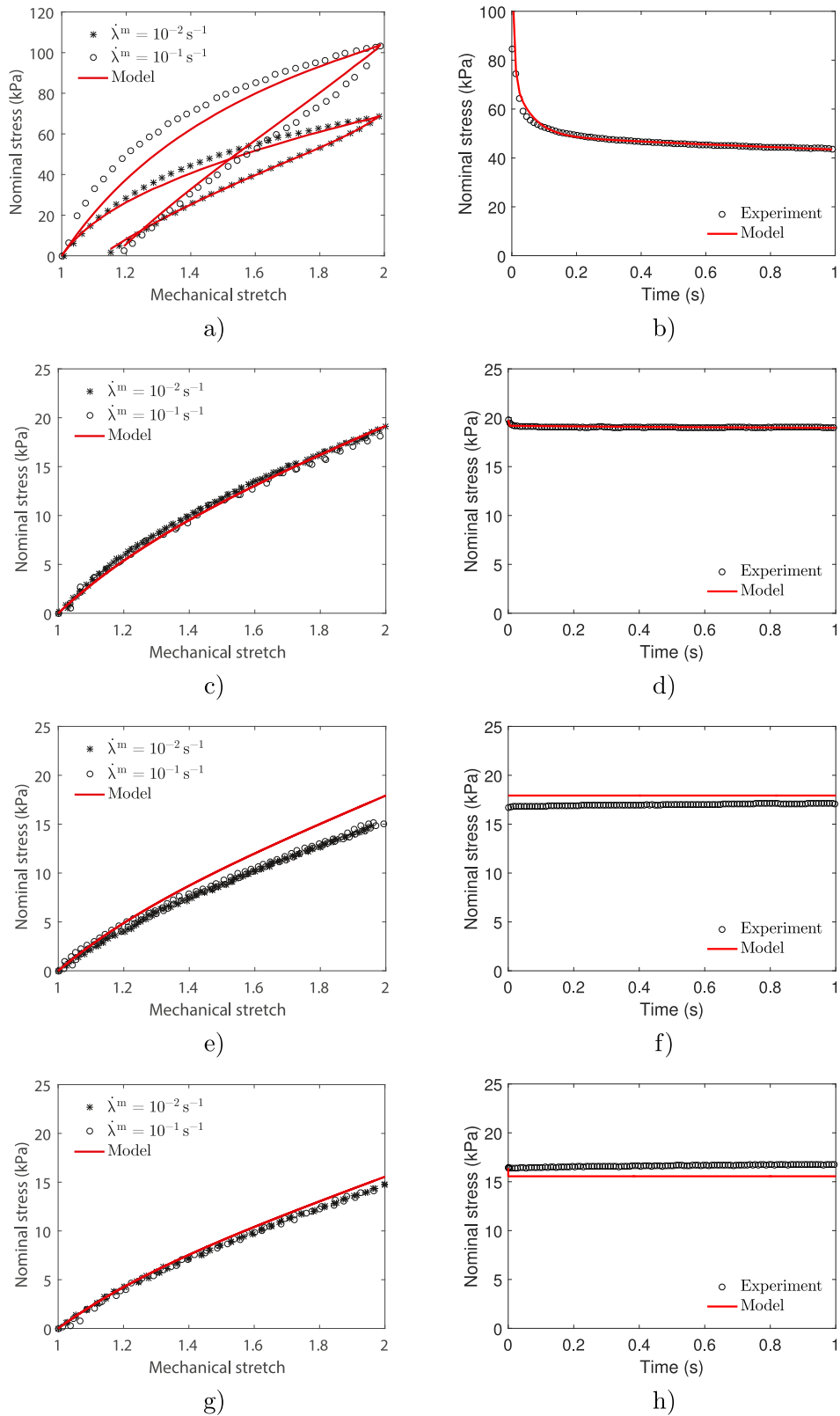


Fig. 17. Calibration of the time-dependent behavior for VHB 4910: a) and b) are virgin; c) and d) fully swollen with n-Pentane; e) and f) fully swollen with o-Xylene; g) and h) fully swollen with Toluene.

Table 6

Measured equilibrium free swelling stretch, and the calibrated polymer-solvent interaction parameter χ for VHB 4910 in various solvents.

	n-Pentane	o-Xylene	Toluene
λ^s	1.49	1.95	1.98
χ	0.631	0.550	0.548

relaxation behavior. This can be seen in Fig. 17d, f and h. However, there is a slight disagreement between the calibrated model and the experimental data for samples fully swollen with o-Xylene, as seen in Fig. 17e and f. Although the vanishing of viscoelastic behavior is accounted for, the stress predicted by the calibrated model is slightly higher than the experimentally obtained values. The possible change in the locking stretch λ_L due to the solvent uptake could be a reason for this discrepancy, however that is not significant enough for us to consider in this work.

The calibrated material parameters are provided in Table 5. Based on the calibrated time-dependent materials parameters, for the samples fully swollen with n-Pentane, we observe a low utilization of viscous mechanisms with the $G_{TD}^{(1)} \approx G_{TD}^{(2)} \approx 0$, and $G_{TD}^{(3)}$ an order of magnitude lower than the values obtained from calibration of virgin behavior. Further, for the samples fully swollen with n-Pentane the relaxation time of the first viscous mechanism exhibits a very fast relaxation, since $\tau^{(1)} \approx 0$ s, while the second and third viscous mechanisms exhibit a very slow relaxation, with $\tau^{(2)} \approx 10^3$ s and $\tau^{(3)} \approx 10^4$ s. For the samples fully swollen with o-Xylene and Toluene, one can observe the apparent absence of all viscous mechanisms since $G_{TD}^{(\gamma)} \approx 0$ relative to the virgin material, along with the instantaneous relaxation observed as $\tau^{(\gamma)} \approx 0$ leading to a time-independent response.

5.3. Calibration of the free swelling behavior

To obtain the polymer-solvent interaction parameter χ , we calibrate the constitutive model to the free swelling data. Following (30), and using the experimentally determined swelling stretch found in Section 3.7.2, along with the material parameters from Table 4, we obtain the χ values for each polymer-solvent combination. The values obtained through calibration are found in Table 6.

5.4. Model summary

The values obtained by calibrating the model for the time-independent behavior display the change in the scaling exponent q with the solvent uptake, while keeping both the initial shear modulus G_0 and locking stretch λ_L fixed. That allows for the constitutive model to reduce back to the same material when dry, while the scaling exponent q originally proposed by Okumura et al. (2016) accounts for the measured change in the effective stiffness due to solvent. Also, as expected, the polymer-solvent interaction parameter χ regulates the degree of swelling, such that as χ decreases the degree of swelling increases.

Calibration of the time-dependent behavior of virgin samples, show utilization of all viscous mechanisms. The calibrated parameters for samples fully swollen with n-Pentane show a very low utilization of viscous mechanisms, since the $G_{TD}^{(\gamma)}$ is at least an order of magnitude lower than those obtained from virgin samples. Additionally, in contrast to the values obtained from the time-dependent calibration of the virgin behavior, for samples fully swollen with o-Xylene and Toluene, we find that $G_{TD}^{(\gamma)} \approx 0$, making all the viscous mechanism insignificant. Further, the relaxation times for all viscous mechanisms is $\tau^{(\gamma)} \approx 0$ when fully swollen in these two solvents, reflecting the apparent instantaneous relaxation of fully swollen VHB 4910. Thus, our constitutive model proved capable of accounting for the apparent vanishing of rate-dependence, hysteresis and stress relaxation behavior of viscoelastic polymeric gels.

6. Conclusion

In this paper we have characterized the viscoelastic response of both dry and fully swollen gels through experimental observations and continuum level modeling. Using VHB 4910 along with three different solvents, n-Pentane, o-Xylene and Toluene, we have measured the mechanical response in (i) quasi-static uniaxial large deformation tension, (ii) uniaxial load-unload at multiple rates, and (iii) stress relaxation; when virgin, fully swollen, and solvent cycled. The most notable result of these experiments being the apparent loss of viscoelasticity in the response due to the uptake of solvent. Additionally, through solvent cycling, our measurements show the reappearance of viscoelasticity, suggesting the process is reversible.

In addition, we have developed a continuum-level constitutive model for viscoelastic polymeric gels. Our model is successfully calibrated against the obtained experimental data, thus proving capable to replicate the major features of viscoelastic gel behavior observed in our experiments. The calibration of our constitutive model showed (i) low utilization of the time-dependent stress contribution for the samples fully swollen in n-Pentane; (ii) almost complete absence of the time-dependent stress contribution for samples fully swollen with o-Xylene and Toluene.

Although not the aim of this study, we have found the failure of the material fully swollen with o-Xylene and Toluene to be occurring at the stretch at which the dry material (both virgin and solvent cycled) is still intact. That is a very interesting result that indicates there is more to learn, however we leave it for future work. Lastly, while we characterized the behavior of a viscoelastic gel when fully swollen, the mechanical response at intermediate degrees of swelling is yet to be determined and is the focus of our future work.

Declaration of competing interest

The authors declare that they have no known competing financial interests or personal relationships that could have appeared to influence the work reported in this paper.

CRediT authorship contribution statement

Nikola Bosnjak: Investigation, Writing - original draft. **Siva Nadimpalli:** Resources, Writing - review & editing. **Dai Okumura:** Writing - review & editing. **Shawn A. Chester:** Supervision, Writing - review & editing.

Acknowledgments

SAC acknowledges support from the [National Science Foundation](#) under grant numbers (CMMI-1463121) and (CMMI-1751520). SN acknowledges support from the National Science Foundation under grant number (CMMI-1652409). DO acknowledges support from the [Japan Society for the Promotion of Science](#) (JSPS) under a Grant-in-Aid for Scientific Research (A) (JP19H00739).

Appendix

A1. Verification of the DIC procedure

To verify the validity of the DIC procedure applied for the testing inside the cylindrical fluid bath, we perform a set of mechanical tests both with and without the fluid bath. First, virgin samples without the fluid bath are tested using the same setup described in [Section 3.1](#). Another set of virgin samples (without swelling in solvent) are tested using the fluid bath full of water using the same procedure. In all cases a prescribed displacement of $u = 20.32 \text{ mm}$ at a rate of $\dot{u} = 20.32 \times 10^{-4} \text{ mm/s}$ is prescribed to the testing machine, which corresponds to a mechanical stretch of $\lambda^m = 2$ at a stretch rate of 10^{-4} s^{-1} . The results presented in [Fig. A1](#) clearly show only a very small difference between the DIC measurements obtained with and without the cylindrical fluid bath, with a maximum error in the measured mechanical stretch of 0.025, which is 1.25%. Therefore we freely use DIC to measure the deformation of samples with the fluid bath.

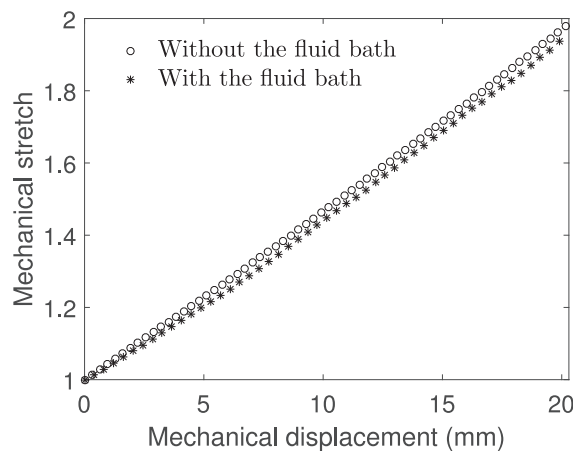


Fig. A1. Comparison of the DIC measured mechanical stretch λ^m on unswollen samples as a function of the mechanical displacement prescribed to the testing machine with and without the fluid bath.

A2. Buoyancy calibration

To account for the effect of buoyancy due to the submerged grip, load train, and sample, we perform a calibration test to determine the change in force per unit depth (N/m) due to buoyancy. This calibration may then be applied to the measured force signal to remove the effect of buoyancy so our reported stress is only what is due to the material response. To perform

the calibration, we keep the sample attached only to the top grip, and do not attach the sample to the bottom grip. The sample, along with the grip and load train is fully submerged inside the fluid bath, with the load cell recording the force due to buoyancy at various depths.

Since the grips and the load train used for a 5 pound load cell are not the same as the one in use for the 100 g load cell, the above mentioned procedure is applied for each of them separately. The measured calibration factor is 1.11 N/m for the 5 pound load cell setup, and 0.64 N/m for the 100 g load cell setup.

References

- Anand, L., 1996. A constitutive model for compressible elastomeric solids. *Comput. Mech.* 18 (5), 339–355.
- Arruda, E.M., Boyce, M.C., 1993. A three-dimensional constitutive model for the large stretch behavior of rubber elastic materials. *J. Mech. Phys. Solids* 41 (2), 389–412.
- Bergström, J., Boyce, M., 1998. Constitutive modeling of the large strain time-dependent behavior of elastomers. *J. Mech. Phys. Solids* 46 (5), 931–954.
- Biot, M.A., 1954. Theory of stress-strain relations in anisotropic viscoelasticity and relaxation phenomena. *J. Appl. Phys.* 25 (11), 1385–1391.
- Chan, E.P., Hu, Y., Johnson, P.M., Suo, Z., Stafford, C.M., 2012. Spherical indentation testing of poroelastic relaxations in thin hydrogel layers. *Soft Matter* 8 (5), 1492–1498.
- Chester, S.A., 2012. A constitutive model for coupled fluid permeation and large viscoelastic deformation in polymeric gels. *Soft Matter* 8 (31), 8223–8233.
- Chester, S.A., Anand, L., 2010. A coupled theory of fluid permeation and large deformations for elastomeric materials. *J. Mech. Phys. Solids* 58 (11), 1879–1906.
- Chester, S.A., Anand, L., 2011. A thermo-mechanically coupled theory for fluid permeation in elastomeric materials: application to thermally responsive gels. *J. Mech. Phys. Solids* 59 (10), 1978–2006.
- Chester, S.A., Di Leo, C.V., Anand, L., 2015. A finite element implementation of a coupled diffusion-deformation theory for elastomeric gels. *Int. J. Solids Struct.* 52, 1–18.
- Cohen, N., McMeeking, R.M., 2019. On the swelling induced microstructural evolution of polymer networks in gels. *J. Mech. Phys. Solids* 125, 666–680.
- Cohen, N., Oren, S.S., deBotton, G., 2017. The evolution of the dielectric constant in various polymers subjected to uniaxial stretch. *Extreme Mech. Lett.* 16, 1–5.
- Crochet, M.J., Naghdi, P.M., 1969. A class of simple solids with fading memory. *Int. J. Eng. Sci.* 7 (12), 1173–1198.
- Davis, B., 1974. Diffusion in polymer gel implants. *Proc. Natl. Acad. Sci.* 71 (8), 3120–3123.
- Deligkaris, K., Tadele, T.S., Olthuis, W., van den Berg, A., 2010. Hydrogel-based devices for biomedical applications. *Sens. Actuators, B* 147 (2), 765–774.
- Doi, M., 2009. Gel dynamics. *Journal of the Physical Society of Japan* 78 (5), 052001–052001.
- Dorfmann, A., Ogden, R., 2005. Nonlinear electroelasticity. *Acta Mech.* 174 (3–4), 167–183.
- Drozdov, A., et al., 2008. Thermo-viscoelastic and viscoplastic behavior of high-density polyethylene. *Int. J. Solids Struct.* 45 (14–15), 4274–4288.
- Drozdov, A.D., 1997. A constitutive model for nonlinear viscoelastic media. *Int. J. Solids Struct.* 34 (21), 2685–2707.
- Drozdov, A.D., Dorfmann, A., 2002. The nonlinear viscoelastic response of carbon black-filled natural rubbers. *Int. J. Solids Struct.* 39 (23), 5699–5717.
- Duda, F.P., Souza, A.C., Fried, E., 2010. A theory for species migration in a finitely strained solid with application to polymer network swelling. *J. Mech. Phys. Solids* 58 (4), 515–529.
- Farshad, M., Le Roux, M., 2005. Compression properties of magnetostrictive polymer composite gels. *Polym. Test* 24 (2), 163–168.
- Ferry, J.D., 1980. *Viscoelastic Properties of Polymers*. John Wiley & Sons.
- Fetters, L., Lohse, D., Richter, D., Witten, T., Zirkel, A., 1994. Connection between polymer molecular weight, density, chain dimensions, and melt viscoelastic properties. *Macromolecules* 27 (17), 4639–4647.
- Flory, P., 1941. Principles of polymer chemistry (cornell univ. press, ithaca, 1953); huggins p. *J. Chem. Phys.* 9, 440.
- Flory, P.J., 1942. Thermodynamics of high polymer solutions. *J. Chem. Phys.* 10 (1), 51–61.
- Flory, P.J., Rehner, J., 1943. Statistical mechanics of cross-linked polymer networks i. rubberlike elasticity. *J. Chem. Phys.* 11 (11), 512–520.
- Flory, P.J., Rehner, J., 1943. Statistical mechanics of cross-linked polymer networks ii. swelling. *J. Chem. Phys.* 11 (11), 521–526.
- Galli, M., Comley, K.S., Shean, T.A., Oyen, M.L., 2009. Viscoelastic and poroelastic mechanical characterization of hydrated gels. *J. Mater. Res.* 24 (3), 973–979.
- Green, M., Tobolsky, A., 1946. A new approach to the theory of relaxing polymeric media. *J. Chem. Phys.* 14 (2), 80–92.
- Hayamizu, K., Aihara, Y., Arai, S., Price, W.S., 1998. Diffusion, conductivity and dsc studies of a polymer gel electrolyte composed of cross-linked poly(γ -butyrolactone and libf4. *Solid State Ionics* 107 (1–2), 1–12.
- Hong, W., Zhao, X., Zhou, J., Suo, Z., 2008. A theory of coupled diffusion and large deformation in polymeric gels. *J. Mech. Phys. Solids* 56 (5), 1779–1793.
- Hossain, M., Vu, D.K., Steinmann, P., 2012. Experimental study and numerical modelling of vhb 4910 polymer. *Comput. Mater. Sci.* 59, 65–74.
- Hossain, M., Vu, D.K., Steinmann, P., 2015. A comprehensive characterization of the electro-mechanically coupled properties of vhb 4910 polymer. *Arch. Appl. Mech.* 85 (4), 523–537.
- Hu, Y., Suo, Z., 2012. Viscoelasticity and poroelasticity in elastomeric gels. *Acta Mech. Solida Sin.* 25 (5), 441–458.
- Hu, Y., Zhao, X., Vlassak, J.J., Suo, Z., 2010. Using indentation to characterize the poroelasticity of gels. *Appl. Phys. Lett.* 96 (12), 121904.
- Huggins, M.L., 1942. Some properties of solutions of long-chain compounds. *J. Phys. Chem.* 46 (1), 151–158.
- Johnson, B., Bauer, J., Niedermaier, D.J., Crone, W., Beebe, D., 2004. Experimental techniques for mechanical characterization of hydrogels at the microscale. *Exp. Mech.* 44 (1), 21–28.
- Kean, Z.S., Hawk, J.L., Lin, S., Zhao, X., Sijbesma, R.P., Craig, S.L., 2014. Increasing the maximum achievable strain of a covalent polymer gel through the addition of mechanically invisible cross-links. *Adv. Mater.* 26 (34), 6013–6018.
- Keshavarz, B., Divoux, T., Manneville, S., McKinley, G.H., 2017. Nonlinear viscoelasticity and generalized failure criterion for polymer gels. *ACS Macro Lett.* 6 (7), 663–667.
- Khan, A.S., Lopez-Pamies, O., 2002. Time and temperature dependent response and relaxation of a soft polymer. *Int. J. Plast.* 18 (10), 1359–1372.
- Khan, A.S., Lopez-Pamies, O., Kazmi, R., 2006. Thermo-mechanical large deformation response and constitutive modeling of viscoelastic polymers over a wide range of strain rates and temperatures. *Int. J. Plast.* 22 (4), 581–601.
- Kleverlaan, M., van Noort, R.H., Jones, I., et al., 2005. Deployment of swelling elastomer packers in shell e&p. In: *SPE/IADC Drilling Conference*. Society of Petroleum Engineers.
- Linder, C., Tkachuk, M., Miehe, C., 2011. A micromechanically motivated diffusion-based transient network model and its incorporation into finite rubber viscoelasticity. *J. Mech. Phys. Solids* 59 (10), 2134–2156.
- Lucantonio, A., Nardinocchi, P., Teresi, L., 2013. Transient analysis of swelling-induced large deformations in polymer gels. *J. Mech. Phys. Solids* 61 (1), 205–218.
- Lutolf, M., Hubbell, J., 2005. Synthetic biomaterials as instructive extracellular microenvironments for morphogenesis in tissue engineering. *Nat. Biotechnol.* 23 (1), 47.
- Miehe, C., Göktepe, S., 2005. A micro-macro approach to rubber-like materials. part ii: the micro-sphere model of finite rubber viscoelasticity. *J. Mech. Phys. Solids* 53 (10), 2231–2258.
- Nam, S., Hu, K.H., Butte, M.J., Chaudhuri, O., 2016. Strain-enhanced stress relaxation impacts nonlinear elasticity in collagen gels. *Proc. Natl. Acad. Sci.* 113 (20), 5492–5497.
- Nguyen, T.D., Qi, H.J., Castro, F., Long, K.N., 2008. A thermoviscoelastic model for amorphous shape memory polymers: incorporating structural and stress relaxation. *J. Mech. Phys. Solids* 56 (9), 2792–2814.

- Okumura, D., Kondo, A., Ohno, N., 2016. Using two scaling exponents to describe the mechanical properties of swollen elastomers. *J. Mech. Phys. Solids* 90, 61–76.
- Partom, Y., Schanin, I., 1983. Modeling nonlinear viscoelastic response. *Polymer Eng. Sci.* 23 (15), 849–859.
- Plazek, D.J., 1965. Temperature dependence of the viscoelastic behavior of polystyrene. *J. Phys. Chem.* 69 (10), 3480–3487.
- Plazek, D.J., 1980. The temperature dependence of the viscoelastic behavior of poly (vinyl acetate). *Polym. J.* 12 (1), 43.
- Rasband, W., 1997–2018. ImageJ. U. S. National Institutes of Health, Bethesda, MD.
- Reese, S., 2003. A micromechanically motivated material model for the thermo-viscoelastic material behaviour of rubber-like polymers. *Int. J. Plast.* 19 (7), 909–940.
- Reese, S., Govindjee, S., 1998. A theory of finite viscoelasticity and numerical aspects. *Int. J. Solids Struct.* 35 (26–27), 3455–3482.
- Rizzieri, R., Baker, F., Donald, A., 2003. A study of the large strain deformation and failure behaviour of mixed biopolymer gels via in situ esem. *Polymer* 44 (19), 5927–5935.
- Ronaldson-Bouchard, K., Ma, S.P., Yeager, K., Chen, T., Song, L., Sirabella, D., Morikawa, K., Teles, D., Yazawa, M., Vunjak-Novakovic, G., 2018. Advanced maturation of human cardiac tissue grown from pluripotent stem cells. *Nature* 556 (7700), 239.
- Rus, D., Tolley, M.T., 2015. Design, fabrication and control of soft robots. *Nature* 521 (7553), 467.
- Smart, J., Williams, J., 1972. A comparison of single-integral non-linear viscoelasticity theories. *J. Mech. Phys. Solids* 20 (5), 313–324.
- Tanaka, T., Fillmore, D.J., 1979. Kinetics of swelling of gels. *J. Chem. Phys.* 70 (3), 1214–1218.
- Urayama, K., Yokoyama, K., Kohjiya, S., 2001. Viscoelastic relaxation of guest linear poly (dimethylsiloxane) in end-linked poly (dimethylsiloxane) networks. *Macromolecules* 34 (13), 4513–4518.
- Valanis, K., 1966. Thermodynamics of large viscoelastic deformations. *J. Math. Phys.* 45 (1–4), 197–212.
- Vinogradov, A., Holloway, F., 1999. Electro-mechanical properties of the piezoelectric polymer pvdf. *Ferroelectrics* 226 (1), 169–181.
- Wang, S., Decker, M., Henann, D.L., Chester, S.A., 2016. Modeling of dielectric viscoelastomers with application to electromechanical instabilities. *J. Mech. Phys. Solids* 95, 213–229.
- Wang, X., Hong, W., 2012. A visco-poroelastic theory for polymeric gels. *Proc. R. Soc. A: Math. Phys. Eng. Sci.* 468 (2148), 3824–3841.
- Webber, R.E., Creton, C., Brown, H.R., Gong, J.P., 2007. Large strain hysteresis and mullins effect of tough double-network hydrogels. *Macromolecules* 40 (8), 2919–2927.
- Williams, M.L., Landel, R.F., Ferry, J.D., 1955. The temperature dependence of relaxation mechanisms in amorphous polymers and other glass-forming liquids. *J. Am. Chem. Soc.* 77 (14), 3701–3707.
- Woerly, S., Doan, V.D., Evans-Martin, F., Paramore, C.G., Peduzzi, J.D., 2001. Spinal cord reconstruction using neurogel implants and functional recovery after chronic injury. *J. Neurosci. Res.* 66 (6), 1187–1197.
- Yohsuke, B., Urayama, K., Takigawa, T., Ito, K., 2011. Biaxial strain testing of extremely soft polymer gels. *Soft Matter* 7 (6), 2632–2638.
- York, A., Dunn, J., Seelecke, S., 2010. Experimental characterization of the hysteretic and rate-dependent electromechanical behavior of dielectric electro-active polymer actuators. *Smart Mater. Struct.* 19 (9), 94014.
- Zamani, V., Pence, T.J., 2017. Swelling, inflation, and a swelling-burst instability in hyperelastic spherical shells. *Int. J. Solids Struct.* 125, 134–149.
- Zhang, S., Ermann, J., Succi, M.D., Zhou, A., Hamilton, M.J., Cao, B., Korzenik, J.R., Glickman, J.N., Vemula, P.K., Glimcher, L.H., et al., 2015. An inflammation-targeting hydrogel for local drug delivery in inflammatory bowel disease. *Science translational medicine* 7 (300), 300ra128–300ra128.
- Zhao, X., Huebsch, N., Mooney, D.J., Suo, Z., 2010. Stress-relaxation behavior in gels with ionic and covalent crosslinks. *J. Appl. Phys.* 107 (6), 63509.